Preprint
UCRL-JC-146186

On the Calculation of Uncertainties for 3-D Time-Dependent Neutral Particle Transport

Peter N. Brown, Keith E. Grant, and Carol S. Woodward

This article was submitted to Journal of Computational Physics

November 21, 2001

DISCLAIMER

On the Calculation of Uncertainties for 3-D Time-Dependent Neutral Particle Transport

Peter N. Brown, Keith E. Grant, and Carol S. Woodward[1]

Center for Applied Scientific Computing, Lawrence Livermore National Laboratory

E-mail: pnbrown@llnl.gov; keg@llnl.gov; cswoodward@llnl.gov

Accurate predictions of uncertainties in computed solutions to neutral particle transport problems are of extreme importance in applications such as shielding design. Often, uncertainties are measured using a Monte Carlo method, where cross section data is sampled at numerous points, the Boltzmann transport simulation code is run with each sampled data point, and the variance of the outputs is quantified. We present an alternative method to this potentially expensive procedure, where solution sensitivities are computed simultaneously with the solution and variances are then computed using these sensitivities. Solutions and sensitivities together take approximately 2 to 3 times longer to solve than solutions alone, but the resulting procedure for uncertainty quantification is far faster than the hundreds of runs often required for the sampling method. Numerical results on a variety of test cases demonstrate that uncertainties measured using the sensitivity analysis approach differ from those computed with the Monte Carlo technique by very small amounts.

1. INTRODUCTION

The ability to model transport of neutral particles, such as neutrons and photons, through matter is of importance to many scientific and engineering applications. These application areas include reactor and shielding design, development of medical radiation treatment, and nuclear well logging. Often deterministic models of these physical systems give rise to the use of the linear Boltzmann transport equation (BTE), an integro-differential equation modeling the particle flux at a given position and energy level through a material in a given direction. Much time and effort has been spent on developing effective solution methods for this problem. See [18] and the references therein for more details.

The BTE has two parameter fields, the scattering and absorbing cross sections, which are usually given as input. The scattering cross section measures how many particles are scattered from a specific energy E' moving in direction Ω' to energy E and direction Ω. The absorbing cross section is a measure of how easily the particles move through the material and is usually related to the optical depth of the given material. Often, these parameters are given as the result of experiments and can suffer from experimental error. These errors result in uncertainty in the simulation solution, and it is critical for many applications to understand the magnitude of this uncertainty.

[1] This work was performed under the auspices of the U.S. Dept. of Energy by University of California, Lawrence Livermore National Laboratory under contract W-7405-ENG-48.

Common techniques for assessing these uncertainties generally require numerous runs of the simulation code with differing values for the cross sections. These techniques use various sampling strategies, such as Latin hypercube, to determine the inputs for these runs, and they use either Bayesian or Frequentist methods for analyzing the collection of solutions and for quantifying the uncertainties [16]. Other methods for quantifying uncertainties compute a solution sensitivity and then use the data covariance to get an estimate of solution uncertainty. The sensitivity analysis approach requires far fewer simulation code runs and less overall time. Sensitivities can easily be computed for BTE solutions as is shown in [20], where both forward and backward in-time methods are used to evaluate the sensitivities.

In this paper, we present our method of computing and using first-order sensitivities to estimate the uncertainty of solutions with respect to the cross sections present in the problem. We apply transformations in order to enhance the ability of the first-order sensitivities to approximate the full sensitivities [14] and compare the results with uncertainties computed using a sampling approach. Results show that the two methods compare well but that the sensitivity analysis approach is far faster than the sampling one.

The paper is organized in seven sections. In the following section we overview the BTE and the multigroup approximation. Section 3 discusses the two uncertainty quantification methods we compare, and Section 4 details our discretization of the BTE. Section 5 discusses the implementation of the sensitivity and sampling approach outlining the mathematical formulation of the sensitivity calculation. Section 6 presents numerical results comparing the two uncertainty estimates for both single group and three-group problems. The last section gives some conclusions.

2. THE BOLTZMANN EQUATION

We begin with the linear time-dependent BTE in a three-dimensional box geometry with general scattering [22]. The spatial domain is the box $\mathcal{D} \equiv \{r = (x, y, z) | a_x \leq x \leq b_x, a_y \leq y \leq b_y, \text{ and } a_z \leq z \leq b_z\}$, the direction variable is $\Omega \in \mathcal{S}^2$, the unit sphere in $\mathbf{R}^3$, the energy variable is $E \in (0, \infty)$, the time variable is t, and the equation in the flux $\psi(r, \Omega, E, t)$ is given by

$$\begin{aligned} &\frac{1}{v(E)}\frac{\partial \psi}{\partial t}(r, \Omega, E, t) + \Omega \cdot \nabla \psi(r, \Omega, E, t) + \sigma(r, E)\psi(r, \Omega, E, t) = \\ &\qquad \int_0^\infty \int_{\mathcal{S}^2} \psi(r, \Omega', E', t)\sigma_s(r, \Omega' \cdot \Omega, E' \to E) d\Omega' dE' + q(r, \Omega, E, t), \\ &\psi(r, \Omega, E, t_0) = \psi^0(r, \Omega, E), \end{aligned} \tag{1}$$

where $\nabla \psi \equiv (\partial\psi/\partial x, \partial\psi/\partial y, \partial\psi/\partial z)$, $v(E)$ is the particle speed, and ψ^0 is the initial state at time $t = t_0$. The functions σ and σ_s are material cross sections, with the σ term representing a loss of particles due to absorption or scattering events resulting in a different energy E' or direction Ω' for the outgoing particle, while the term involving σ_s represents a source of particles due to scattering from other directions and energies into the energy E and direction Ω. The function $q(r, \Omega, E, t)$ represents an external source of particles.

Boundary conditions must also be specified to make (1) well-posed. For simplicity, we consider only Dirichlet boundary conditions in which the incident flux is specified on a face. Specifically, we consider boundary conditions of the form

$$\psi(r, \Omega, E, t) = \psi_B(r, \Omega, E, t) \text{ for all } t \geq t_0, \, r \in \partial\mathcal{D} \text{ and } \Omega \in \mathcal{S}^2 \text{ with } \vec{n}(r) \cdot \Omega < 0, \tag{2}$$

where $\vec{n}(r)$ is the outward pointing unit normal at $r \in \partial\mathcal{D}$. Other options include a reflecting condition on a face, or so-called white boundary conditions that couple all the incident and outgoing fluxes on a face.

A semi-discretization of (1) can be obtained using a *multigroup* discretization of the energy E (see, e.g., [18]). In the multigroup approach, the energy E is restricted to a finite interval partitioned into subintervals, or "groups":

$$E_{max} = E_0 > E_1 > \cdots > E_G = E_{min}. \tag{3}$$

The equation (1) is then averaged over each group $E_g < E < E_{g-1}$ and the cross sections σ and σ_s are approximated by certain "flux-weighted averages" to maintain linearity. This yields the following semi-discretization of (1):

$$\frac{1}{v_g}\frac{\partial \psi_g}{\partial t}(r,\Omega,t) + \Omega \cdot \nabla \psi_g(r,\Omega,t) + \sigma_g(r)\psi_g(r,\Omega,t) = \sum_{g'=0}^{G-1} \int_{\mathcal{S}^2} \sigma_{s,g,g'}(r,\Omega' \cdot \Omega)\psi_{g'}(r,\Omega',t)d\Omega' + q_g(r,\Omega,t), \tag{4}$$

for $g = 0, \cdots, G-1$, where

$$\psi_g(r,\Omega,t) \equiv \int_{E_{g+1}}^{E_g} \psi(r,\Omega,E,t)dE \quad \text{and} \quad q_g(r,\Omega,t) \equiv \int_{E_{g+1}}^{E_g} q(r,\Omega,E,t)dE.$$

Alternatively, one can derive similar equations by using a piecewise constant finite element discretization in energy.

When solving (4), for each g the flux $\psi_g(r,\Omega,t)$ is expanded in surface harmonics according to

$$\psi_g(r,\Omega,t) = \sum_{n=0}^{\infty} \sum_{m=-n}^{n} \phi_{g,n}^m(r,t) Y_n^m(\Omega),$$

where $Y_n^m(\Omega)$ is a surface harmonic and

$$\phi_{g,n}^m(r) \equiv \int_{\mathcal{S}^2} \psi_g(r,\Omega) Y_n^m(\Omega) d\Omega$$

is the $(n,m)^{th}$ moment of ψ_g.

Given ψ_g above, one is able to rewrite the scattering integral in the form

$$\int_{\mathcal{S}^2} \sigma_{s,g,g'}(r,\Omega' \cdot \Omega)\psi_{g'}(r,\Omega')d\Omega' = \sum_{n=0}^{\infty} \sigma_{s,g,g',n}(r) \sum_{m=-n}^{n} \phi_{g',n}^m(r) Y_n^m(\Omega), \tag{5}$$

where the $\sigma_{s,g,g',n}$ are given by

$$\sigma_{s,g,g',n}(r) \equiv 2\pi \int_{-1}^{1} \sigma_{s,g,g'}(r,\mu_0) P_n(\mu_0) d\mu_0,$$

and where μ_0 is the cosine of the scattering angle. The infinite series in (5) is truncated to a finite number of terms, with a maximum value, N_s, for n. The group total cross section is defined as

$$\sigma_g(r) \equiv \sigma_{a,g}(r) + \sum_{g'=0}^{G-1} \sigma_{s,g,g',0}(r) \text{ , with } \sigma_{a,g} \equiv \int_{E_{g+1}}^{E_g} \sigma_a(r,E)dE, \tag{6}$$

for the absorption cross section $\sigma_a(r,E)$. Thus, we can write the multigroup equations as

$$\frac{1}{v_g}\frac{\partial \psi_g}{\partial t}(r,\Omega,t) + \Omega \cdot \nabla \psi_g(r,\Omega,t) + \sigma_g(r)\psi_g(r,\Omega,t) = \sum_{g'=0}^{G-1} \sum_{n=0}^{N_s} \sigma_{s,g',g,n}(r) \sum_{m=-n}^{n} \phi_{g',n}^m(r) Y_n^m(\Omega) + q_g(r,\Omega,t), \tag{7}$$

for $g = 0, \cdots, G-1$.

3. UNCERTAINTY QUANTIFICATION

In this section we describe how sensitivities can be used to estimate uncertainties in the context of solving the neutron transport equation (1). To simplify the presentation, we restrict here to the steady state mono-energetic case (i.e., one energy group) and assume that the cross sections are constant in space along with isotropic scattering. Hence, we have

$$\sigma = \sigma_a + \sigma_s,$$

with the scalars σ_a and σ_s representing the absorption and isotropic scattering cross sections, and (1) reduces to

$$\begin{aligned} &(\Omega \cdot \nabla + \sigma)\psi(r,\Omega) = \sigma_s \int_{\mathcal{S}^2} \psi(r,\Omega')d\Omega' + q(r,\Omega), \\ &\psi(r,\Omega) = \psi_B(r,\Omega) \text{ for all } r \in \partial\mathcal{D} \text{ and } \Omega \in \mathcal{S}^2 \text{ with } \vec{n}(r)\cdot\Omega < 0. \end{aligned} \tag{8}$$

For many problems, a typical output quantity of interest is a detector count of the generic form

$$d(\psi, \sigma_a) \equiv \int_{S^2}\int_D \sigma_a \psi(r,\Omega)drd\Omega, \tag{9}$$

for some spatial region D. We refer to the function $d(\psi, \sigma_a)$ as a *detector response function*. A related quantity that can also be of interest is what we call the *integrated particle flux* over the detector region, namely

$$\tilde{\psi} \equiv \int_{S^2}\int_D \psi(r,\Omega)drd\Omega. \tag{10}$$

In real problems, the cross sections come from experimental data and so have some uncertainty associated with them. The main question we want to try and answer is the following: *What is the uncertainty in the integrated particle flux and detector response function caused by the uncertainties in the cross sections?*

We compare two approaches to answering this question: a direct calculation of the uncertainty using a full Monte Carlo sampling approach, and an estimate of the uncertainty obtained using sensitivity analysis.

3.1. The Full Monte Carlo Sampling Approach

We begin by assuming the (σ_a, σ_s) values come from a population with a given probability distribution having means $\hat{\sigma}_a$ and $\hat{\sigma}_s$, and covariance matrix $C(\sigma_a, \sigma_s)$. Let

$$(\sigma_{a,1}, \sigma_{s,1}), \ldots, (\sigma_{a,n}, \sigma_{s,n})$$

be a random sample of size n from this population. We then solve equation (8) for each pair, and let ψ_i denote the solution corresponding to $(\sigma_{a,i}, \sigma_{s,i})$. Let $d_i = d(\psi_i, \sigma_{a,i})$ denote the corresponding detector response. Then

$$\bar{d} \equiv \frac{1}{n}\sum_{i=1}^{n} d_i \quad \text{and} \quad s_d^2 \equiv \frac{1}{n-1}\sum_{i=1}^{n}(d_i - \bar{d})^2 \tag{11}$$

are sample estimates of the true mean detector response and its variance, which we will assume represents the uncertainty in the detector response function. The problem with the full Monte Carlo sampling approach is that the sample size n needed to ensure that $\bar{d}$ and s_d^2 are good estimates is typically prohibitively large, given that we must solve (8) n times. We next describe how to use sensitivity analysis as a way to estimate these quantities at a reduced cost.

3.2. The Sensitivity Analysis Approach

In this approach, we again assume that we have a random sample of size n from the (σ_a, σ_s) population. However, instead of solving (8) n times, first let

$$\bar{\sigma}_a \equiv \frac{1}{n}\sum_{i=1}^{n}\sigma_{a,i} \quad \text{and} \quad \bar{\sigma}_s \equiv \frac{1}{n}\sum_{i=1}^{n}\sigma_{s,i} \tag{12}$$

be the corresponding sample means. We then solve (8) using $\sigma_a = \bar{\sigma}_a$ and $\sigma_s = \bar{\sigma}_s$, denoting the solution by $\psi(\bar{\sigma}_a, \bar{\sigma}_s)$ and letting $\tilde{d} = d(\psi(\bar{\sigma}_a, \bar{\sigma}_s), \bar{\sigma}_a)$.

In the sensitivity analysis approach, we use a first order Taylor series for $\psi(\sigma_a, \sigma_s)$ to approximate the dependence of ψ on the parameters σ_a and σ_s. That is, we use

$$\psi(\sigma_a, \sigma_s) \approx \psi(\bar{\sigma}_a, \bar{\sigma}_s) + \frac{\partial\psi}{\partial\sigma_a}(\bar{\sigma}_a, \bar{\sigma}_s)\cdot(\sigma_a - \bar{\sigma}_a) + \frac{\partial\psi}{\partial\sigma_s}(\bar{\sigma}_a, \bar{\sigma}_s)\cdot(\sigma_s - \bar{\sigma}_s). \tag{13}$$

The derivatives $\partial\psi/\partial\sigma_a$ and $\partial\psi/\partial\sigma_s$ are called the *sensitivities* of ψ with respect to σ_a and σ_s. Equations for these derivatives can be obtained by differentiating (8) with respect to σ_a and σ_s separately, giving (recalling that $\sigma = \sigma_a + \sigma_s$)

$$\begin{aligned} &(\Omega\cdot\nabla + \sigma)\,\frac{\partial\psi}{\partial\sigma_a} = \sigma_s\int_{\mathcal{S}^2}\frac{\partial\psi}{\partial\sigma_a}(r,\Omega')d\Omega' - \psi(r,\Omega), \\ &\frac{\partial\psi}{\partial\sigma_a}(r,\Omega,) = 0 \text{ for all } r\in\partial\mathcal{D} \text{ and } \Omega\in\mathcal{S}^2 \text{ with } \vec{n}(r)\cdot\Omega < 0, \end{aligned} \tag{14}$$

and

$$\begin{aligned} &(\Omega\cdot\nabla + \sigma)\,\frac{\partial\psi}{\partial\sigma_s} = \sigma_s\int_{\mathcal{S}^2}\frac{\partial\psi}{\partial\sigma_s}(r,\Omega')d\Omega' + \int_{S^2}\psi(r,\Omega')d\Omega' - \psi(r,\Omega), \\ &\frac{\partial\psi}{\partial\sigma_s}(r,\Omega,) = 0 \text{ for all } r\in\partial\mathcal{D} \text{ and } \Omega\in\mathcal{S}^2 \text{ with } \vec{n}(r)\cdot\Omega < 0. \end{aligned} \tag{15}$$

We then solve these equations using $\sigma_a = \bar{\sigma}_a$, $\sigma_s = \bar{\sigma}_s$, and $\psi = \psi(\bar{\sigma}_a, \bar{\sigma}_s)$.

Next, we want to use the above Taylor series approximation to obtain an estimate for the variance $s_{\bar{d}}^2$ in (11). However, we don't have $\bar{d}$ in (11), only the estimate $\tilde{d} = d(\psi(\bar{\sigma}_a, \bar{\sigma}_s), \bar{\sigma}_a)$. From the definition of $d(\psi, \sigma_a)$, we can write

$$d(\psi(\sigma_a, \sigma_s), \sigma_a) \approx \tilde{d} + \frac{\partial d}{\partial\sigma_a}(\bar{\sigma}_a, \bar{\sigma}_s)\cdot(\sigma_a - \bar{\sigma}_a) + \frac{\partial d}{\partial\sigma_s}(\bar{\sigma}_a, \bar{\sigma}_s)\cdot(\sigma_s - \bar{\sigma}_s),$$

where

$$\begin{aligned} &\frac{\partial d}{\partial\sigma_a}(\sigma_a, \sigma_s) \equiv \sigma_a\int_{S^2}\int_D\frac{\partial\psi}{\partial\sigma_a}drd\Omega + \int_{S^2}\int_D\psi drd\Omega \text{ , and} \\ &\frac{\partial d}{\partial\sigma_s}(\sigma_a, \sigma_s) \equiv \sigma_a\int_{S^2}\int_D\frac{\partial\psi}{\partial\sigma_s}drd\Omega. \end{aligned} \tag{16}$$

Using $\tilde{d}$ as an estimate of $\bar{d}$, we have

$$\begin{aligned} \bar{d} - \tilde{d} &= \frac{1}{n}\sum_{i=1}^{n}\left[d(\psi(\sigma_{a,i}, \sigma_{s,i}), \sigma_{a,i}) - d(\psi(\bar{\sigma}_a, \bar{\sigma}_s), \bar{\sigma}_a)\right] \\ &\approx \frac{1}{n}\sum_{i=1}^{n}\left[\frac{\partial d}{\partial\sigma_a}(\bar{\sigma}_a, \bar{\sigma}_s)\cdot(\sigma_{a,i} - \bar{\sigma}_a) + \frac{\partial d}{\partial\sigma_s}(\bar{\sigma}_a, \bar{\sigma}_s)\cdot(\sigma_{s,i} - \bar{\sigma}_s)\right] \\ &= 0. \end{aligned}$$

Thus, we will use $\bar{d} = \tilde{d}$, since this is true to first order. Next, we define the vectors

$$\Delta\sigma_a \equiv \begin{pmatrix} \sigma_{a,1} - \bar{\sigma}_a \\ \vdots \\ \sigma_{a,n} - \bar{\sigma}_a \end{pmatrix}, \quad \Delta\sigma_s \equiv \begin{pmatrix} \sigma_{s,1} - \bar{\sigma}_s \\ \vdots \\ \sigma_{s,n} - \bar{\sigma}_s \end{pmatrix} \quad \text{and} \quad \Delta d \equiv \begin{pmatrix} d_1 - \bar{d} \\ \vdots \\ d_n - \bar{d} \end{pmatrix}.$$

Then we have

$$\Delta d \approx \begin{pmatrix} \frac{\partial d}{\partial \sigma_a}(\bar{\sigma}_a, \bar{\sigma}_s) \cdot (\sigma_{a,1} - \bar{\sigma}_a) + \frac{\partial d}{\partial \sigma_s}(\bar{\sigma}_a, \bar{\sigma}_s) \cdot (\sigma_{s,1} - \bar{\sigma}_s) \\ \vdots \\ \frac{\partial d}{\partial \sigma_a}(\bar{\sigma}_a, \bar{\sigma}_s) \cdot (\sigma_{a,n} - \bar{\sigma}_a) + \frac{\partial d}{\partial \sigma_s}(\bar{\sigma}_a, \bar{\sigma}_s) \cdot (\sigma_{s,n} - \bar{\sigma}_s) \end{pmatrix} = [\Delta\sigma_a, \Delta\sigma_s] \cdot \begin{pmatrix} \frac{\partial d}{\partial \sigma_a}(\bar{\sigma}_a, \bar{\sigma}_s) \\ \frac{\partial d}{\partial \sigma_s}(\bar{\sigma}_a, \bar{\sigma}_s) \end{pmatrix}.$$

Using these relationships, we can write

$$s_d^2 = \frac{1}{n-1}\Delta d^T \Delta d \approx \frac{1}{n-1}\left(\frac{\partial d}{\partial \sigma_a}(\bar{\sigma}_a, \bar{\sigma}_s), \frac{\partial d}{\partial \sigma_s}(\bar{\sigma}_a, \bar{\sigma}_s)\right) \begin{bmatrix} \Delta\sigma_a^T \\ \Delta\sigma_s^T \end{bmatrix} [\Delta\sigma_a, \Delta\sigma_s] \begin{pmatrix} \frac{\partial d}{\partial \sigma_a}(\bar{\sigma}_a, \bar{\sigma}_s) \\ \frac{\partial d}{\partial \sigma_s}(\bar{\sigma}_a, \bar{\sigma}_s) \end{pmatrix},$$

or

$$s_d^2 \approx \hat{s}_d^2 \equiv c^T V c, \tag{17}$$

where

$$c \equiv \begin{pmatrix} \frac{\partial d}{\partial \sigma_a}(\bar{\sigma}_a, \bar{\sigma}_s) \\ \frac{\partial d}{\partial \sigma_s}(\bar{\sigma}_a, \bar{\sigma}_s) \end{pmatrix} \text{ and } V \equiv \frac{1}{n-1}\begin{bmatrix} \Delta\sigma_a^T \Delta\sigma_a & \Delta\sigma_a^T \Delta\sigma_s \\ \Delta\sigma_s^T \Delta\sigma_a & \Delta\sigma_s^T \Delta\sigma_s \end{bmatrix}.$$

The matrix V is an approximation to the covariance matrix $C(\sigma_a, \sigma_s)$ defined earlier. The derivatives in the vector c are evaluated using (16) and the calculated sensitivities found by solving equations (14) and (15) for $\sigma_a = \bar{\sigma}_a$ and $\sigma_s = \bar{\sigma}_s$. These ideas can also be applied in a similar way to estimate uncertainties in the integrated particle flux (10).

Of course, the error $e = s_d^2 - \hat{s}_d^2$ depends upon how well the linear Taylor series approximations used above describe the true nonlinear behavior of the uncertainties. In the numerical studies performed in a later section, we will attempt to explore the limits of acceptability for the linear sensitivity analysis approach. One could also extend this linear approach to a higher order method in the natural way. For example, a quadratic approach would require three additional solves for the extra sensitivities and would generally be more accurate, but it would most likely still be much less expensive than the full Monte Carlo sampling approach.

3.3. Extensions

We briefly describe extensions of our simplified example to problems involving multiple energy groups and materials, higher order scattering, and time dependence. For multiple energy groups, the scalars σ_a and σ_s are replaced by matrices of size $G \times G$. For example, the total cross section σ is replaced by the matrix

$$\Sigma = \Sigma_a + \hat{\Sigma}_{s,0}, \tag{18}$$

where

$$\Sigma_a \equiv \text{diag}(\sigma_{a,0}, \ldots, \sigma_{a,G-1}) \quad \text{and} \quad \hat{\Sigma}_{s,0} \equiv \text{diag}\left(\sum_{g'=0}^{G-1} \sigma_{s,1,g',0}, \ldots, \sum_{g'=0}^{G-1} \sigma_{s,G,g',0}\right).$$

Next, the scattering cross section σ_s is replaced by moment matrices $\Sigma_{s,n}$ defined by

$$\Sigma_{s,n} \equiv \begin{pmatrix} \sigma_{s,0,0,n} & \cdots & \sigma_{s,0,G-1,n} \\ \vdots & \ddots & \vdots \\ \sigma_{s,G-1,0,n} & \cdots & \sigma_{s,G-1,G-1,n} \end{pmatrix} \tag{19}$$

for $n = 0, 1, \ldots, N_s$. Furthermore, for each material in the problem, there is a set of matrices as in (18) and (19). In a typical problem, one may want to calculate the uncertainty associated with all of the parameters in these matrices for all materials, or perhaps just a subset. Our methods for estimating uncertainty work well on these harder problems. In the numerical results section, we give an example problem using three energy groups to illustrate this fact. Finally, adding time dependence means solving the original time-dependent problem along with similar equations for all of the now time-dependent sensitivities.

4. DISCRETIZATION OF THE 3-D PROBLEM

We give a brief overview of our discretization approach in space and direction, as this has been extensively described in our earlier work ([1] and [4]). We begin with a short subsection on notation, and then proceed to the discrete form of the Boltzmann equation.

4.1. Notation

For matrices $A \in \mathbf{R}^{m\times n}$ and $B \in \mathbf{R}^{k\times l}$, the *Kronecker* (or *tensor*) *product* of A and B is the $mk \times nl$ matrix denoted by

$$A \otimes B \equiv \begin{pmatrix} a_{11}B & \cdots & a_{1n}B \\ \vdots & \ddots & \vdots \\ a_{m1}B & \cdots & a_{mn}B \end{pmatrix},$$

where $A = (a_{ij})$. Kronecker products have many interesting properties. We list here the ones relevant to our discussion:

- If A and B are nonsingular, then $A \otimes B$ is nonsingular with $(A \otimes B)^{-1} = A^{-1} \otimes B^{-1}$,
- $(A \otimes B)^T = A^T \otimes B^T$,
- Given matrices A, B, C, and D, $(A \otimes B) \cdot (C \otimes D) = AC \otimes BD$, as long as both sides of the equation make sense,
- $(A + B) \otimes C = A \otimes C + B \otimes C$, and
- $A \otimes (B + C) = A \otimes B + A \otimes C$.

4.2. Quadrature Rules

The specific quadrature rules we consider for approximating integrals on $\mathcal{S}^2$ employ the standard symmetry assumptions. Following Carlson and Lathrop [6], we consider quadrature rules of the form

$$\int_{\mathcal{S}^2} \psi(\Omega) d\Omega \approx \sum_{\ell=1}^{L} w_\ell \psi(\Omega_\ell), \tag{20}$$

where $\Omega_\ell \equiv (\mu_\ell, \eta_\ell, \xi_\ell)$, for all $\ell = 1, \ldots, L$, with $L = \nu(\nu + 2)$ and ν is the number of direction cosines ($\nu = 2, 4, 6, \ldots$). See [4] for more details.

4.3. The Petrov-Galerkin Spatial Discretization

We next consider the spatial discretization of the system (7). For each group g and each direction Ω_ℓ, we use a *Petrov-Galerkin* finite-element method for the solution of the problem

$$\begin{cases} \frac{1}{v}\frac{\partial}{\partial t}\psi + \Omega\cdot\nabla\psi + \sigma\psi = f \text{ in } \mathcal{D}, \\ \psi(r) = \psi_B(r) \text{ for all } r \in \partial\mathcal{D} \text{ with } \vec{n}(r)\cdot\Omega < 0, \end{cases} \tag{21}$$

where $\Omega = (\mu,\eta,\xi) \in \mathcal{S}^2$ is fixed and equal to one of the above quadrature points, $\sigma = \sigma_g$, and $v = v_g$ (although we suppress the ℓ and g subscripts to simplify notation), $\mathcal{D}$ is the spatial domain defined earlier, and $\vec{n}(r)$ is the outward pointing unit normal at $r \in \partial\mathcal{D}$. The functions f, g, and σ are assumed known.

We first discretize $\mathcal{D}$ into zones in the natural way, and define

$$\begin{aligned} &\Delta x_i = x_i - x_{i-1} \text{ for } i = 1,\ldots,M, \quad \Delta y_j = y_j - y_{j-1} \text{ for } j = 1,\ldots,J, \text{ and} \\ &\Delta z_k = z_k - z_{k-1} \text{ for } k = 1,\ldots,K, \end{aligned}$$

and define $r_{ijk} = (x_i, y_j, z_k)$. Also define $\Delta r_{ijk} \equiv \Delta x_i \Delta y_j \Delta z_k$. The $\{r_{ijk}\}$ are referred to as *nodes*, and function values at these points are called *nodal values*. Assume that σ and f have constant values on each *zone*

$$\mathcal{Z}_{ijk} \equiv \{r | x_{i-1} < x < x_i, y_{j-1} < y < y_j, z_{k-1} < z < z_k\},$$

denoted by σ_{ijk} and f_{ijk}, respectively. Function values that are constant on zones will be referred to as *zone-centered* values. We use ψ_{ijk} to denote the approximation to $\psi(r_{ijk})$, the true solution at r_{ijk}, and use piecewise continuous trilinear elements to approximate ψ. We then test against piecewise constant functions in space. Following the development given in [4], there are $(M+1)(J+1)(K+1)$ unknowns ψ_{ijk}. There are MJK zonal equations, and $MK + JM + JK + M + J + K + 1$ boundary equations.

Writing the discretized system in matrix notation, we first have the discrete flux vector

$$\Psi \in \mathbf{R}^{(M+1)(J+1)(K+1)},$$

defined for all nodes ordered in the natural way. Next, define diagonal matrices $\Delta x \equiv \text{diag}(\Delta x_1,\ldots,\Delta x_M)$, with Δy and Δz similarly, and define the matrices $D_M \in \mathbf{R}^{M\times(M+1)}$ and $S_M \in \mathbf{R}^{M\times(M+1)}$ by

$$D_M \equiv \begin{pmatrix} -1 & 1 & & \\ & \ddots & \ddots & \\ & & -1 & 1 \end{pmatrix} \text{ and } S_M \equiv \frac{1}{2}\begin{pmatrix} 1 & 1 & & \\ & \ddots & \ddots & \\ & & 1 & 1 \end{pmatrix}. \tag{22}$$

In a similar way, define the matrices D_J, S_J, D_K, and S_K. Let $\Sigma \equiv \text{diag}(\sigma_{111},\ldots,\sigma_{MJK}) \in \mathbf{R}^{MJK}$, and define the matrices C_x, C_y, C_z, and S by

$$\begin{aligned} &C_x \equiv S_K \otimes S_J \otimes \Delta x^{-1} D_M, \quad C_y \equiv S_K \otimes \Delta y^{-1} D_J \otimes S_M, \\ &C_z \equiv \Delta z^{-1} D_K \otimes S_J \otimes S_M, \quad \text{and } S \equiv S_K \otimes S_J \otimes S_M. \end{aligned}$$

The matrices C_x, C_y, and C_z represent the discretized versions of the differentiation operators $\partial/\partial x$, $\partial/\partial y$, $\partial/\partial z$, respectively, and S represents an averaging matrix taking nodal vectors into zone-centered vectors. With these definitions, it is possible to write the MJK zone-centered equations in the unknown Ψ as

$$S\dot{\Psi} + (C + \Sigma S)\Psi = F, \tag{23}$$

where $C \equiv \mu C_x + \eta C_y + \xi C_z$, and $F \equiv (f_{ijk}) \in \mathbf{R}^{MJK}$ and $\dot{\Psi}$ denotes the time derivative of Ψ.

To isolate the boundary values, first note that for a direction vector Ω with all its components positive, ψ satisfies a Dirichlet condition for all $r = r_{0jk}$, r_{i0k}, or r_{ij0}, i.e., for an r on any one of the three faces $x = x_0$, $y = y_0$, or $z = z_0$. For any such Ω, letting Ψ_B be a vector of the same dimension as Ψ whose possibly nonzero entries are values of $\psi_B(r, \Omega)$ at all the boundary points, the discrete boundary conditions can be written as $E_{000}(\Psi - \Psi_B) = 0$, where

$$E_{000} \equiv \begin{pmatrix} e_{0K}^T \otimes I_{J+1} \otimes I_{M+1} \\ (0, I_K) \otimes e_{0J}^T \otimes I_{M+1} \\ (0, I_K) \otimes (0, I_J) \otimes e_{0M}^T \end{pmatrix},$$

with the vectors e_{0J} and e_{0K} having the natural interpretations. There are different E matrices for the other possible quadrature points. In all, there are eight different E_{ijk} matrices, with $i = 0$ or M, $j = 0$ or J, and $k = 0$ or K.

At this point it is necessary to introduce the dependence of Ψ, Ψ_B, and the matrix C on the quadrature point Ω and group index g. For a given $\Omega = \Omega_\ell$ and g, the vector Ψ is really $\Psi_{g,\ell}$, $\Psi_B = \Psi_{B,g,\ell}$, and the matrix $C = C_\ell$, for the subscript ℓ corresponding to that Ω. Then the matrix representation of the discrete version of (21) can be written as

$$\begin{pmatrix} S \\ 0 \end{pmatrix} \dot{\Psi}_{g,\ell} + H_{g,\ell} \Psi_{g,\ell} = \begin{pmatrix} F_{g,\ell} \\ B_\ell \Psi_{B,g,\ell} \end{pmatrix}, \text{ where } H_{g,\ell} \equiv \begin{pmatrix} C_\ell + \Sigma_g S \\ B_\ell \end{pmatrix}, \tag{24}$$

with $B_\ell = E_{ijk}$ for the appropriate choice of i, j, k, and $C_\ell = \mu_\ell C_x + \eta_\ell C_y + \xi_\ell C_z$. Note that $H_{g,\ell}$ operates on nodal vectors.

4.4. The Discrete Ordinates Method

Continuing the matrix development of the overall discretization of the BTE, we begin by defining discretized representations of the operations of taking moments of the flux. As operators on zone-centered vectors, these are easily seen to be given by the $MJK \times LMJK$ matrices

$$L_{n,m} \equiv \left(\, w_1 Y_n^m(\Omega_1) I \, \middle| \, w_2 Y_n^m(\Omega_2) I \, \middle| \cdots \middle| \, w_L Y_n^m(\Omega_L) I \, \right). \tag{25}$$

Similarly, we define the $LMJK \times MJK$ matrices

$$L_{n,m}^+ \equiv \begin{pmatrix} Y_n^m(\Omega_1) I \\ \vdots \\ Y_n^m(\Omega_L) I \end{pmatrix}, \tag{26}$$

where $I = I_{MJK}$. We also will find it useful to define the grouped matrices L_n and L_n^+, where

$$L_n = \begin{pmatrix} L_{n,-n} \\ \vdots \\ L_{n,n} \end{pmatrix} \text{ and } L_n^+ = \left(L_{n,-n}^+, \cdots, L_{n,n}^+ \right),$$

and also the further grouped matrices

$$L^N = \begin{pmatrix} L_0 \\ \vdots \\ L_N \end{pmatrix} \text{ and } L^{N,+} = \left(L_0^+, \cdots, L_N^+ \right).$$

To represent the source term, define the zone-centered vector $Q \equiv (q_{ijk\ell}) \in \mathbf{R}^{LMJK}$, where $q_{ijk\ell} \equiv q(r_{ijk}, \Omega_\ell)$. For the boundary terms, define the block diagonal matrices B and C by

$$B \equiv \text{diag}(B_1, \ldots, B_L) \text{ and } C \equiv \text{diag}(C_1, \ldots, C_L),$$

and let

$$\begin{aligned}
\Sigma_{s,g,g',n} &\equiv I_{2n+1} \otimes \hat{\Sigma}_{s,g,g',n}, \quad \text{where} \\
&\quad \hat{\Sigma}_{s,g,g',n} \equiv \text{diag}(\sigma_{s,g,g',n,111}, \ldots, \sigma_{s,g,g',n,MJK}), \quad n = 0, 1, \ldots, \\
\bar{Z} &\equiv I_L \otimes Z, \text{ where } Z \equiv \begin{pmatrix} I_{MJK} \\ 0 \end{pmatrix} \in \mathbf{R}^{(M+1)(J+1)(K+1) \times MJK} \\
\bar{Z}_B &\equiv I_L \otimes Z_B, \text{ where} \\
&\quad Z_b \equiv \begin{pmatrix} 0 \\ I_{(M+1)(J+1)(K+1)-MJK} \end{pmatrix} \in \mathbf{R}^{(M+1)(J+1)(K+1) \times (M+1)(J+1)(K+1)-MJK} \\
\bar{\Sigma} &\equiv I_L \otimes \Sigma, \text{ and} \\
\bar{S} &\equiv I_L \otimes S.
\end{aligned} \tag{27}$$

The matrix $\bar{Z}$ injects zone-centered vectors into the nodal vector space, and the matrix $\bar{S}$ averages nodal vectors to obtain zone-centered ones. Note that $\bar{Z}^T \bar{Z} = I$ and $\bar{Z}^T \bar{Z}_B = 0$. Using the above matrices, define the matrix H_g by

$$H_g \equiv \text{diag}(H_{g,1}, \ldots, H_{g,L}) = \bar{Z}(C + \bar{\Sigma}_g \bar{S}) + \bar{Z}_B B. \tag{28}$$

The matrices $\bar{Z}$ and $\bar{Z}_B$ are needed since H_g operates on nodal vectors, while the scattering matrix operates on zone-centered vectors. (Recall that f was assumed to be zone-centered in the development of the Petrov-Galerkin method discussed earlier.) If we assume only $N_s + 1$ terms in the scattering operator, then the complete discretization of (1)–(2) (modulo the time t) can be written in the compact form

$$\begin{aligned}
&\frac{1}{v_g} \bar{Z} \bar{S} \dot{\Psi}_g + H_g \Psi_g = \bar{Z} \sum_{g'=0}^{G-1} \sum_{n=0}^{N_s} L_n^+ \Sigma_{s,g,g',n} L_n \bar{S} \Psi_{g'} + F_g, \\
&\Psi_g(t_0) = \Psi_g^0, \quad g = 0, \cdots, G-1,
\end{aligned} \tag{29}$$

with $F_g \equiv \bar{Z} Q_g + \bar{Z}_B B \Psi_{B,g}$ and the $\dot{\Psi}_g$ denoting the time derivative of Ψ_g.

Next, if we define

$$\mathbf{\Psi} \equiv \begin{pmatrix} \Psi_0 \\ \Psi_1 \\ \vdots \\ \Psi_{G-1} \end{pmatrix}, \quad \mathbf{F} \equiv \begin{pmatrix} F_0 \\ F_1 \\ \vdots \\ F_{G-1} \end{pmatrix}, \quad \mathbf{\Sigma_s} \equiv \begin{pmatrix} \Sigma_{s,0,0}^{N_s} & \cdots & \Sigma_{s,0,G-1}^{N_s} \\ \vdots & \ddots & \vdots \\ \Sigma_{s,G-1,0}^{N_s} & \cdots & \Sigma_{s,G-1,G-1}^{N_s} \end{pmatrix},$$

where $\Sigma_{s,gg'}^{N_s} \equiv \text{diag}\,(\Sigma_{s,g,g',0}, \cdots, \Sigma_{s,g,g',N_s})$, and define $\mathbf{S} \equiv I_G \otimes \bar{S}$, $\mathbf{Z} \equiv I_G \otimes \bar{Z}$, $\mathbf{H} \equiv \text{diag}(H_1, H_2, \cdots, H_G)$, $\mathbf{L}^+ \equiv I_G \otimes L^{N_s,+}$, $\mathbf{L} \equiv I_G \otimes L^{N_s}$, and $\mathbf{V} \equiv \text{diag}(v_0, \cdots, v_{G-1}) \otimes I_{MJKL}$, then (29) can be written as

$$\begin{aligned}
&\mathbf{V}^{-1} \mathbf{Z} \mathbf{S} \dot{\mathbf{\Psi}} + \mathbf{H} \mathbf{\Psi} = \mathbf{Z} \mathbf{L}^+ \mathbf{\Sigma_s} \mathbf{L} \mathbf{S} \mathbf{\Psi} + \mathbf{F}, \\
&\mathbf{\Psi}(t_0) = \mathbf{\Psi}^0.
\end{aligned} \tag{30}$$

Since the boundary equations do not involve derivatives of the unknown $\mathbf{\Psi}$, this system is properly referred to as a differential-algebraic system of equations (DAEs), and in the next section we describe our solution procedure.

5. IMPLEMENTATION

In this section, we discuss some of the particular methods employed in our implementations of the two uncertainty techniques. For either case, we formulate the BTE discrete system as a differential-algebraic equation (DAE). After

describing this approach, we show how the solution method is easily extended to compute sensitivities. Lastly, we will detail our sampling approach for the cross section parameters.

5.1. DAE Solution Procedure

We write the DAE system (30) in the form

$$F(t, \mathbf{\Psi}, \dot{\mathbf{\Psi}}) = 0, \tag{31}$$

where

$$F(t, \mathbf{\Psi}, \dot{\mathbf{\Psi}}) \equiv \mathbf{V}^{-1}\mathbf{ZS}\dot{\mathbf{\Psi}} + \mathbf{H\Psi} - \mathbf{ZL}^{+}\mathbf{\Sigma_s LS\Psi} - \mathbf{F}.$$

The time integration of the DAE system (30) is accomplished via the IDA (Implicit Differential/Algebraic Equation) solver developed by Hindmarsh and Taylor ([11]). This software package is a parallel code written in the C language for the solution of general initial value DAE systems. IDA uses Backward Differential Formula (BDF) methods to perform the time integration. The BDF methods are variable in order and step size and are also implicit. This method results in a linear system of the form

$$F(t, \mathbf{\Psi}, \alpha\mathbf{\Psi} + \mathbf{\Upsilon}) = 0$$

that must be solved at each time step. Here, $\alpha = \alpha_0/\Delta t_n$ is a constant that changes whenever the step size or order changes, $\mathbf{\Upsilon}$ is a vector that depends on the solution $\mathbf{\Psi}$ at past times, and t, $\mathbf{\Psi}$, and α are evaluated at t_n. From the definition of F, it follows that the above linear system has the form

$$(\mathbf{H} + \alpha\mathbf{V}^{-1}\mathbf{ZS} - \mathbf{ZL}^{+}\mathbf{\Sigma_s LS})\mathbf{\Psi} = \mathbf{F} - \mathbf{V}^{-1}\mathbf{ZS\Upsilon}. \tag{32}$$

As an example, using the BDF method of order 1 (i.e., Backward Euler) for the time integration, the linear system to solve is

$$(\mathbf{H} + (\Delta t_n\mathbf{V})^{-1}\mathbf{ZS} - \mathbf{ZL}^{+}\mathbf{\Sigma_s LS})\mathbf{\Psi}^n = \mathbf{F}^n + (\Delta t_n\mathbf{V})^{-1}\mathbf{ZS\Psi}^{n-1}. \tag{33}$$

Within IDA, system (32) is solved via a preconditioned GMRES iteration. We employ three types of preconditioners to use in the solution of (32). The first is based on the so-called "sweeping procedure" typically used to invert the discrete $\Omega \cdot \nabla + \sigma$ operator represented here by the matrix $\mathbf{H}$, the second combines this with a Diffusion Synthetic Acceleration (DSA) approach, while the third uses a block Gauss-Seidel approach in energy. As the focus in this paper is on the calculation of solution sensitivities, the specific details of these preconditioners are not discussed here. We refer the interested reader to [5].

5.2. Computation of Sensitivities

Using similar notation as above, we can write time-dependent versions of (14) and (15) as a system of equations for the scaled sensitivities $S_a = \tilde{\sigma}_a \frac{\partial \Psi}{\partial \sigma_a}$ and $S_s = \tilde{\sigma}_s \frac{\partial \Psi}{\partial \sigma_s}$, where $\tilde{\sigma}_a$ and $\tilde{\sigma}_s$ are nominal values of the cross sections. We then discretize as above to give linear equations for the sensitivities

$$\frac{\partial F}{\partial \Psi} S_i + \frac{\partial F}{\partial \dot{\Psi}} \dot{S}_i + \frac{\partial F}{\partial \sigma_i} = 0, \tag{34}$$

where i can be either a or s for absorbing or scattering cross sections, respectively. We calculate the solution to these equations with the sensitivity version of IDA [17]. This software augments the DAE system given in (31) with the linear systems (34) so that a single DAE system is solved giving the BTE solution as well as the sensitivities of that solution to each of the opacities.

Letting

$$\mathbf{Y}(\mathbf{t}) \equiv \begin{pmatrix} \mathbf{\Psi(t)} \\ \mathbf{S_a(t)} \\ \mathbf{S_s(t)} \end{pmatrix}, \quad \mathbf{M}(\mathbf{t}, \mathbf{Y}, \dot{\mathbf{Y}}, \sigma_\mathbf{a}, \sigma_\mathbf{s}) \equiv \begin{pmatrix} F \\ \frac{\partial F}{\partial \Psi} S_a + \frac{\partial F}{\partial \dot{\Psi}} \dot{S_a} + \frac{\partial F}{\partial \sigma_a} \\ \frac{\partial F}{\partial \Psi} S_s + \frac{\partial F}{\partial \dot{\Psi}} \dot{S_s} + \frac{\partial F}{\partial \sigma_s} \end{pmatrix},$$

we have the new DAE system,

$$\mathbf{M}(\mathbf{t}, \mathbf{Y}, \dot{\mathbf{Y}}, \sigma_\mathbf{a}, \sigma_\mathbf{s}) = 0.$$

The derivatives of F are approximated by finite-difference techniques,

$$\frac{\partial F}{\partial \Psi} S_a \approx \frac{F(t, \Psi + \delta_\Psi S_a, \dot{\Psi}, \sigma_a, \sigma_s) - F(t, \Psi - \delta_\Psi S_a, \dot{\Psi}, \sigma_a, \sigma_s)}{2\delta_\Psi},$$

and similarly for the derivatives of F with respect to $\dot{\Psi}$ and the S_i. One could also use automatic differentiation techniques, and future releases of SensIDA will provide basic interfaces to the automatic differentiation software, ADIC [3].

The sensitivity version of IDA chooses time steps for the BDF methods so that accuracy is insured for both BTE solutions as well as the sensitivities. As in IDA, implicit problems are solved at each time step using GMRES and making use of the preconditioners that are used for the state variables.

In the steady state case, we employ the Krylov Inexact Newton SOLver, KINSOL, and its sensitivity variant [23, 9] to solve for the BTE system solution and its sensitivities.

5.3. Latin Hypercube Sampling

We now develop details of our implementation of Monte Carlo uncertainty quantification. In order to accurately and simultaneously sample the probability distributions of multiple model parameters, we motivate our handling of random number generation, sampling method, and covariance management. Simultaneous random sampling of the probability distribution of model parameters is conceptually simple and provides a mechanism for estimating the fully nonlinear dependencies of model output on parameter uncertainty. Efficient and accurate implementation is, however, more demanding.

In creating our random sampling sets below, we have used the Park and Miller [21] random number generator embedded within the Bays and Durham [2] shuffle algorithm. Park and Miller have defined a "minimal standard" linear congruential algorithm having a long period before repetition occurs, with minimal serial correlations, and implementable on any machine having integer arithmetic of 32 or more bits. Bays and Durham have provided a shuffling algorithm for removing residual serial correlations from generated numbers. Our implementation of the Park and Miller algorithm was verified by comparison with the published 10,000th number generated from a seed of one. The final routine was checked for randomness via scatter plots, lag correlation analysis, and spectral analysis.

For a given number of Monte Carlo runs, N, the simple random expectation for the standard deviation of the mean, $\bar{s}$ is $\bar{s} = s/\sqrt{(N)}$, where s is the sample variance of the output result. The efficiency of a Monte Carlo sampling method can be defined as the ratio $\bar{s}/\hat{s}$ for the same N runs, where $\hat{s}$ is the observed variance in the mean result. Under this definition, simple random sampling has been found to be much less efficient than more systematic sampling methods [10, 7, 8]. Latin Hypercube Sampling (LHS) is a particularly effective and widely used variance reducing scheme [19, 14, 13]. Moreover, LHS accomplishes this variance reduction without biasing the expected means or distributions.

To create a Latin Hypercube Sample set, the cumulative probability distribution ($0 < p < 1$) for each of K parameters was divided into N equal probability strata. For the one-group studies reported here, values of 50 and 2 were used for N and K, respectively. For the three-group problem, N and K were 50 and 9, respectively. K random permutations of the integers from 1 to N were formed, creating an N by K combination matrix $\tilde{B}$. Each of the N

rows of this matrix constitutes a sampling vector that randomly selects a single stratum interval from the probability distribution of each of the K parameters to be varied.

This combination process and choice of N ensures that each parameter is sampled, over ± 2 standard deviations with each of the N probability intervals for a given parameter being used exactly once. Because of these features, for relatively small sampling sets (e.g., 50 to 100 samples), LHS yields much more representative approximate distributions than would have been expected with simple random sampling. This property results in reduced variance among the model result means and distributions obtained using successive sampling sets. It has been found that using LHS can reduce the number of runs required to obtain a given variance by a factor of 10 compared with simple random sampling [8].

Two issues related to correlations between the K parameters arise in the sampling process described above. The first is that the sampling process may create inadvertent and unwanted correlations between parameters. The second is that there may be actual correlations between parameters that should be taken into account. Both of these issues can be handled within the context of LHS sampling [12, 13], however, in the cases below we have assumed the independence of different cross sections and used the methodology of this section only to minimize the rank correlation between parameters.

The first step in managing correlations between parameters is to transform the combination matrix $\tilde{B}$, created as described above, element by element into a corresponding score matrix $\tilde{R}$ which can be numerically manipulated. Iman and Connover [12] suggested use of the van der Waerden scores

$$r = G^{-1}\left(\frac{i}{N+1}\right),\ i = 1 \ldots N$$

as the transformation between $\tilde{B}$ and $\tilde{R}$, where G^{-1} is the inverse cumulative normal distribution. It is then assumed that, following sampling, the $N \times K$ score matrix $\tilde{R}$ has a $K \times K$ correlation matrix $\tilde{C}_s$. As described above, $\tilde{C}_s$ may differ from the identity matrix because of non-negligible correlations unintentionally introduced by the sampling process. Because correlation matrices are symmetric positive definite, the Cholesky decomposition of $\tilde{C}_s$ can be found:

$$\tilde{C}_s = QQ^T.$$

Similarly, if there is a target correlation between parameters to be imposed, the target correlation matrix C_t can be Cholesky decomposed:

$$C_t = PP^T.$$

A transformation S can then be defined such that

$$SQQ^TS^T = PP^T,$$

which, by inspection, has the solution

$$S = PQ^{-1}.$$

The matrix $R = \tilde{R}S^T$ will have the desired target correlation. A new sample combination matrix B having the same rank correlation as R is then obtained as the rank ordering of R.

To complete the generation of a sample set, a random probability is uniformly chosen within each interval selected. Thus,

$$p = p_i(1-u) + p_{i+1}u,$$

where p_i and p_{i+1} are the probabilities at the lower and upper limits of a cumulative probability interval and u is a uniform random number such that $0 < u < 1$. Finally, the K separate probabilities of a sample set are converted

into coordinates using an inverse cumulative normal transformation [13], giving parameter permutations in units of standard deviations to be applied to the parameter means.

6. NUMERICAL TESTS

In this section we demonstrate the effectiveness of using the sensitivity analysis approach to calculating uncertainties on several representative test problems. The three mono-energetic test problems represent three of the typical problem regimes for transport: a highly diffusive regime involving many collisions with little absorption; a thin regime in which the medium is almost transparent to the neutrons; and a highly absorbing regime. In a problem involving a range of energies, the most energetic neutrons may essentially stream through the material medium, while the least energetic undergo many collisions before being absorbed.

6.1. Simple Mono-Energetic Test Problem Results

Our first set of test problems are mono-energetic steady-state problems in three parameter regimes of interest: thick and diffusive (i.e., many scattering collisions with little absorption), thin (few collisions), and thick with absorption (many collisions with significant absorption). The problem domain is a cube of length 20cm on a side for all three problems, with an internal source region that is also a cube of length 10cm centered in the larger cube. The source is identically constant within this smaller region and zero outside. Vacuum Dirichlet boundary conditions are assumed on all faces of the cube.

6.1.1. Diffusive Problem

For the diffusive problem, the cross sections used throughout the problem are $\sigma_a = 0.01\text{cm}^{-1}$ and $\sigma_s = \sigma_{s,0} = 9.99\text{cm}^{-1}$. The source strength is $0.1\text{n} \cdot \text{cm}^{-2} \cdot \text{s}^{-1}$. This problem appropriately requires DSA/sweeping-based preconditioning. The spatial mesh is uniform of size $M = J = K = 20$ and an S_2 quadrature rule is used (i.e., eight directions). Figures 1, 2, and 3 show sample plots of the solution and the scaled sensitivities. Note the inverted color map that appears in Figure 2. This results because an increase in the absorption cross section will decrease the overall flux, and hence this sensitivity will have negative values.

6.1.2. Thin Problem

For the thin problem, the cross sections used throughout the problem are $\sigma_a = 0.00005\text{cm}^{-1}$ and $\sigma_s = \sigma_{s,0} = 0.00005\text{cm}^{-1}$. The source strength is again $0.1\text{n} \cdot \text{cm}^{-2} \cdot \text{s}^{-1}$. This problem only requires sweeping-based preconditioning. The spatial mesh is uniform of size $M = J = K = 20$ and an S_6 quadrature rule is used (i.e., 48 directions). Figures for this problem and the next are similar to those for the diffusive problem and so are omitted.

6.1.3. Thick Problem

For the thick problem, the cross sections used are $\sigma_a = 0.05\text{cm}^{-1}$ and $\sigma_s = \sigma_{s,0} = 0.05\text{cm}^{-1}$. The source strength is again $0.1\text{n} \cdot \text{cm}^{-2} \cdot \text{s}^{-1}$. This problem also only requires sweeping-based preconditioning. The spatial mesh is uniform of size $M = J = K = 20$ and an S_6 quadrature rule is used (i.e., 48 directions).

6.2. Analysis of One-Group Problems

6.2.1. General Concepts

We now compare the variances of results obtained with the nonlinear model via Monte Carlo Latin Hypercube Sampling (MC) with those obtained from the linear (i.e., first-order) sensitivity (LS) expansions calculated via (13), (10), and (17). In performing this analysis, it has been assumed that the absorption and scattering cross sections are independent. Although the correlation management technique of Section 5.3 is general, we have used it only to minimize inadvertent rank correlations between cross sections under the assumption that all cross sections are independent.

For model parameters sampled from Gaussian distributions, the diagnostic distributions from the LS method are necessarily Gaussian via the linearity of (13) — the sum of individual Gaussian distributions being Gaussian [15]. In

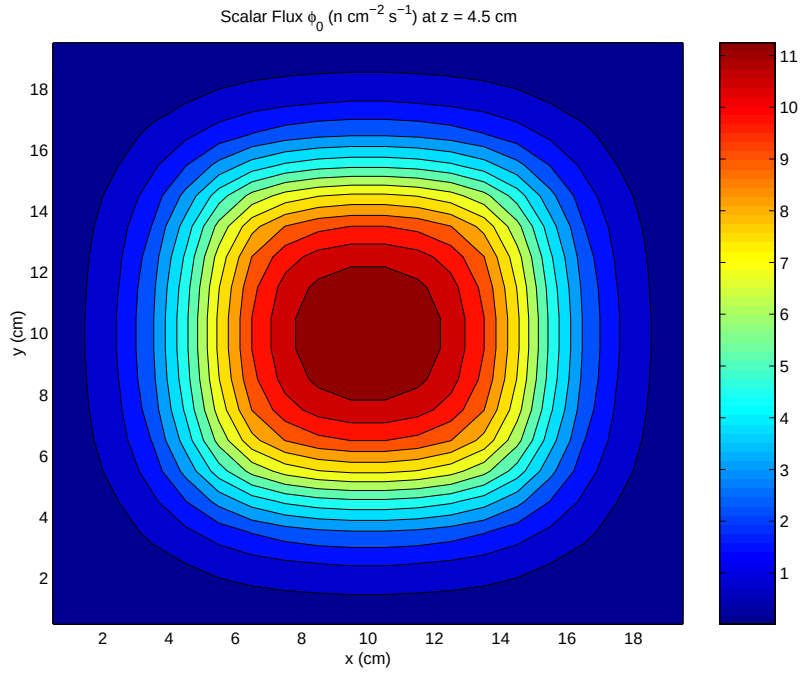

FIG. 1. Scalar flux ϕ_0 for diffusive test problem

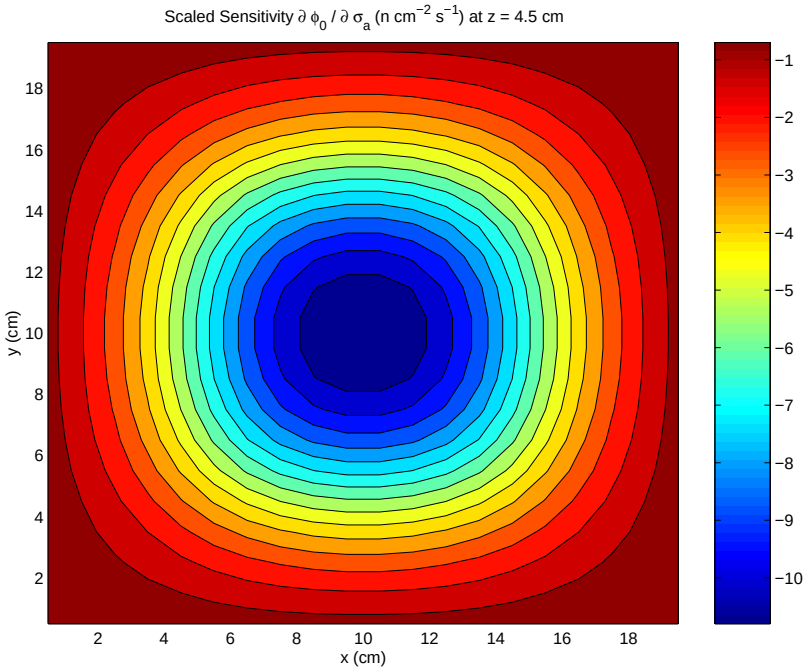

FIG. 2. Scaled sensitivity $\partial\phi_0/\partial\sigma_a$ of scalar flux for diffusive test problem

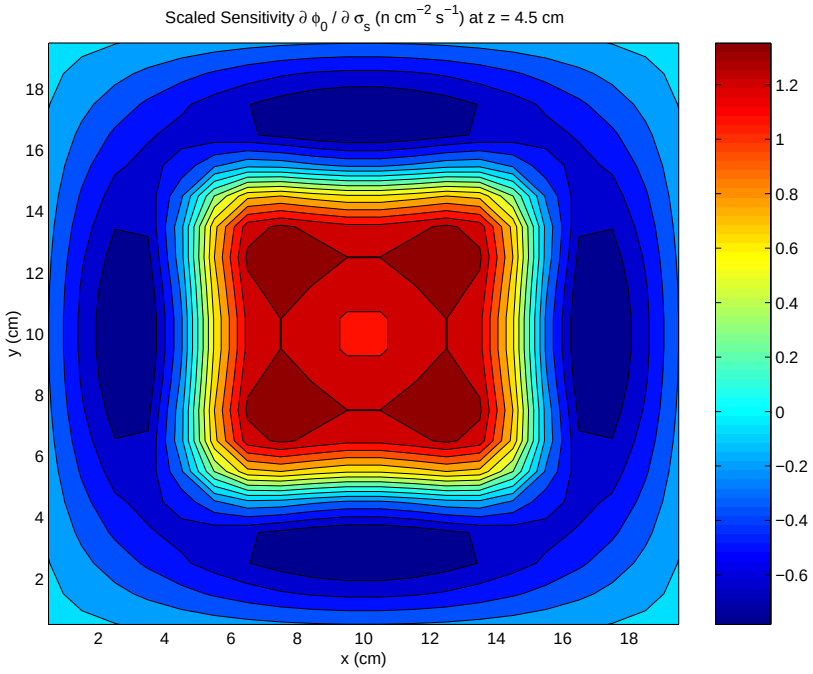

FIG. 3. Scaled sensitivity $\partial\phi_0/\partial\sigma_s$ of scalar flux for diffusive test problem

contrast, the distributions from the MC method are not necessarily Gaussian, although, in some cases, a transformation may make them nearly so [14, 15]. As the discussion below for the diffusion test problem elucidates, the range of applicability of first-order sensitivities may be substantially extended by careful consideration of the physics of their application.

In considering the physics of the BTE, increasing σ_a should increase absorption, correspondingly decreasing the integrated flux, $\tilde{\psi}$, defined by (10). The global detector response of (9), however, also depends linearly on σ_a. Thus, the detector count defined by (9) must display the significantly nonlinear asymptotic behavior of going to zero both for very small and for large σ_a. Therefore, $\tilde{\psi}$, because of its monotonic dependence on σ_a, should better match the linear expansion of (13). Based on this observation, the analyses (below) of the steady-state tests were done in terms of $\tilde{\psi}$ rather than d.

6.2.2. Thin Test Problem

For the thin test problem, 100 MC runs were done for each of two uncertainty assumptions: one in which σ_a and σ_s were sampled from Gaussian distributions for 10% standard deviations relative to the respective nominal values and one in which the error was assumed to be 30%. In Table 1 we give the standard deviation for parameter sampling, number of runs, nominal value for $\tilde{\psi}$, mean values and standard deviations of $\tilde{\psi}$ for Monte Carlo LHS sampling (MC) and linear sensitivity (LS) respectively, and percentage difference of the LS standard deviation relative to that from MC. The scatter-plot in Figure 4a shows the correlation in $\tilde{\psi}$ calculated from LS with respect to that from MC for an assumed cross section error of 30%. The variation of the difference between the two estimates as a function of σ_a is shown in Figure 4b, with the additional variation in σ_s shown by the dot color.

It is clear from Table 1 that in both the 10% and 30% error cases the linear sensitivities provide accurate estimates of output uncertainty for the thin test problem. The differences between the LS and MC cases, shown in Figure 4b,

TABLE 1

Comparison of means and standard deviations for the one-group thin test problem. $\tilde{\psi}_{MC}$ were evaluated via full Monte Carlo runs. $\tilde{\psi}_{LS}$ were evaluated via use of (13) and (10). The last column gives the percentage difference in the standard deviations estimated via the LS method relative to the standard deviation from the MC method.

Sample Std Dev	Number Samples	Nominal $\tilde{\psi}$	Mean $\tilde{\psi}_{MC}$	Mean $\tilde{\psi}_{LS}$	Std Dev $\tilde{\psi}_{MC}$	Std Dev $\tilde{\psi}_{LS}$	Percent %Δ in Std Dev
10%	100	4.0712e+3	4.0712e+3	4.0712e+3	1.4188e-1	1.4186e-1	-0.0138
30%	100	4.0712e+3	4.0712e+3	4.0712e+3	4.2577e-1	4.2557e-1	-0.0463

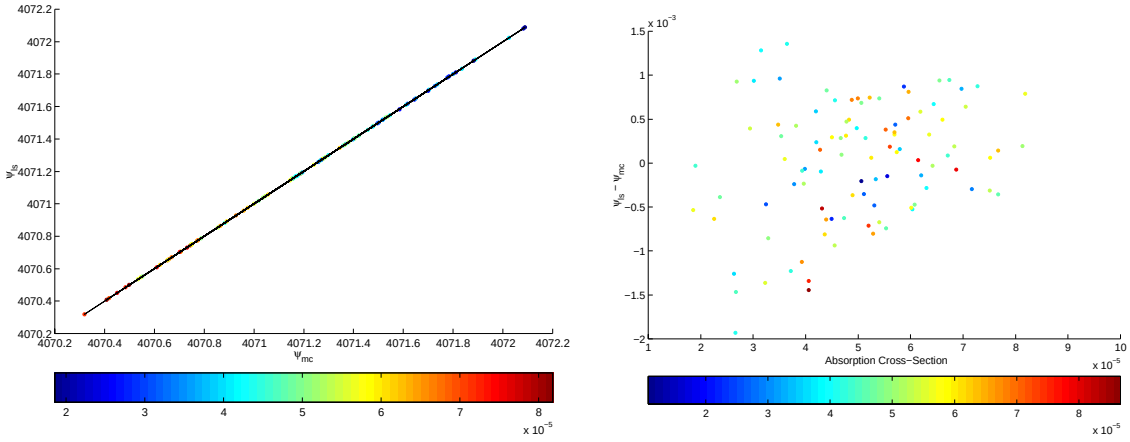

FIG. 4. Run-by-run correlation and differences between $\tilde{\psi}_{MC}$ and $\tilde{\psi}_{LS}$ for the thin test problem with an assumed cross section error of 30%. In (a), the dot color shows σ_a. In (b), the differences are ploted relative to σ_a and the dot color shows σ_s.

appear to be randomly distributed, consistent with the interpretation of these differences as consisting of numerical noise.

6.2.3. Thick Test Problem

For the thick test problem, 150 LHS runs were done for each of two uncertainty assumptions: one in which σ_a and σ_s were sampled from Gaussian distributions for 10% standard deviations relative to the respective nominal values, and one in which the error was assumed to be 30%. In Table 2 we give the sampling standard deviation, number of runs, nominal value for $\tilde{\psi}$, mean values and standard deviations of $\tilde{\psi}$ for Monte Carlo LHS sampling (MC) and linear sensitivity (LS) respectively, and percentage difference of the LS standard deviation relative to that from MC. The scatter-plot in Figure 5a shows the correlation in $\tilde{\psi}$ calculated from LS with respect to that from MC for an assumed cross section error of 30%. The variation of the difference between the two estimates as a function of σ_a is shown in Figure 5b, with the additional variation in σ_s shown by the dot color.

It is clear from Table 2 that in both the 10% and 30% error cases that linear sensitivities provide accurate estimates of output uncertainty for the thick test problem. For the scenario of 30% assumed error, the correlation between the results for LS and MC are displayed in Figure 5a. In contrast to results for the thin problem, Figure 5a shows visible deviation of the LS from the MC cases for large deviations of σ_a. The differences between the LS and MC cases,

TABLE 2

Comparison of means and standard deviations for the one-group thick test problem. $\tilde{\psi}_{MC}$ were evaluated via full Monte Carlo runs. $\tilde{\psi}_{LS}$ were evaluated via use of (13) and (10). The last column gives the percentage difference in the standard deviations estimated via the LS method relative to the standard deviation from the MC method.

Sample Std Dev	Number Samples	Nominal $\tilde{\psi}$	Mean $\tilde{\psi}_{MC}$	Mean $\tilde{\psi}_{LS}$	Std Dev $\tilde{\psi}_{MC}$	Std Dev $\tilde{\psi}_{LS}$	Percent %Δ in Std Dev
10%	150	3.3800e+3	3.3820e+3	3.3796e+3	1.0982e+2	1.0937e+2	-0.404
30%	150	3.3800e+3	3.4013e+3	3.3787e+3	3.3730e+2	3.2811e+2	-2.724

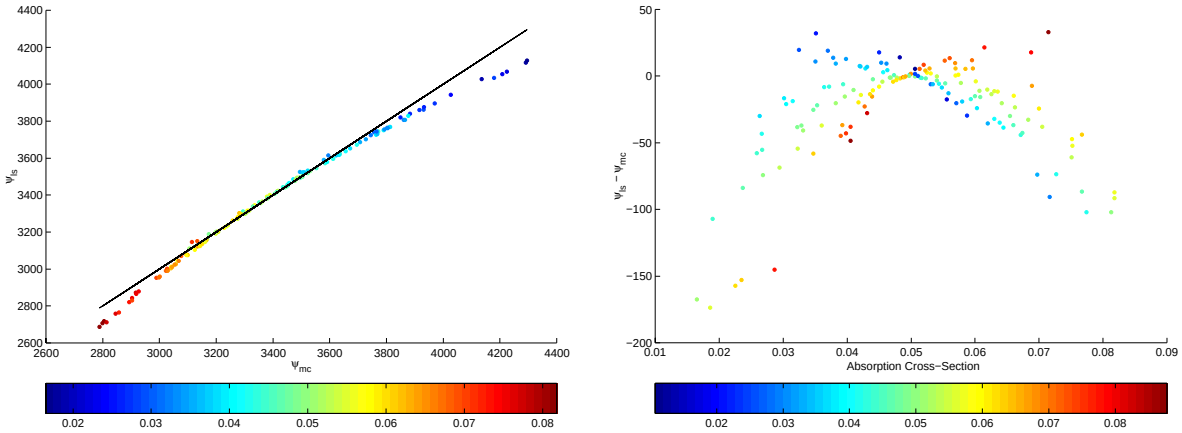

FIG. 5. Run-by-run correlation and differences between $\tilde{\psi}_{MC}$ and $\tilde{\psi}_{LS}$ for the thick test problem with an assumed cross section error of 30%. In (a), the dot color shows σ_a. In (b), the differences are ploted relative to σ_a and the dot color shows σ_s.

shown in Figure 5b, now show a definite dependence on σ_a. Despite this dependence, the estimates of the standard deviation about the nominal value for the MC and LS treatments remain within 3% of each other.

6.2.4. Diffusive Test Problem

For the diffusive test problem 200 LHS runs were done, in which σ_a and σ_s were sampled from Gaussian distributions for 10%, 20%, and 30% standard deviations relative to their respective nominal values. Table 3 gives the statistics accumulated for these runs. For the 20% and 30% sampling standard deviations, it is apparent that there are substantial differences in the $\tilde{\psi}$ standard deviations estimated by the LS method compared to the MC method. For the 30% case, Figure 6 confirms the nature of these deviations, the dependence of $\tilde{\psi}$ on σ_a is clearly nonlinear. It would be premature, however, to conclude that the LS method cannot be accurately applied to this problem.

To some approximation, it is plausible to consider that the integrated particle flux, $\tilde{\psi}$, from (10) will be proportional to the mean free path for absorption. The mean free path for absorption in turn should be inversely proportional to σ_a. This would suggest either performing the analysis in terms of $\tilde{\psi}^{-1}$ or in resampling the parameter error in terms of inverse cross sections and doing a new set of Monte Carlo runs. We have chosen the former as the quicker to implement.

TABLE 3

Comparison of means and standard deviations for the one-group diffusive test problem. $\tilde{\psi}_{MC}$ were evaluated via full Monte Carlo runs. $\tilde{\psi}_{LS}$ were evaluated via use of (13) and (10). The last column gives the percentage difference in the standard deviations estimated via the LS method relative to the standard deviation from the MC method.

Sample Std Dev	Number Samples	Nominal $\tilde{\psi}$	Mean $\tilde{\psi}_{MC}$	Mean $\tilde{\psi}_{LS}$	Std Dev $\tilde{\psi}_{MC}$	Std Dev $\tilde{\psi}_{LS}$	Percent %Δ in Std Dev
10%	200	3.3435e+4	3.3637e+4	3.3435e+4	3.0330e+3	2.9289e+3	-3.43
20%	200	3.3435e+4	3.4295e+4	3.3435e+4	6.7670e+3	5.8579e+3	-13.4
30%	200	3.3435e+4	3.5667e+4	3.3435e+4	1.3227e+4	8.7868e+3	-33.6

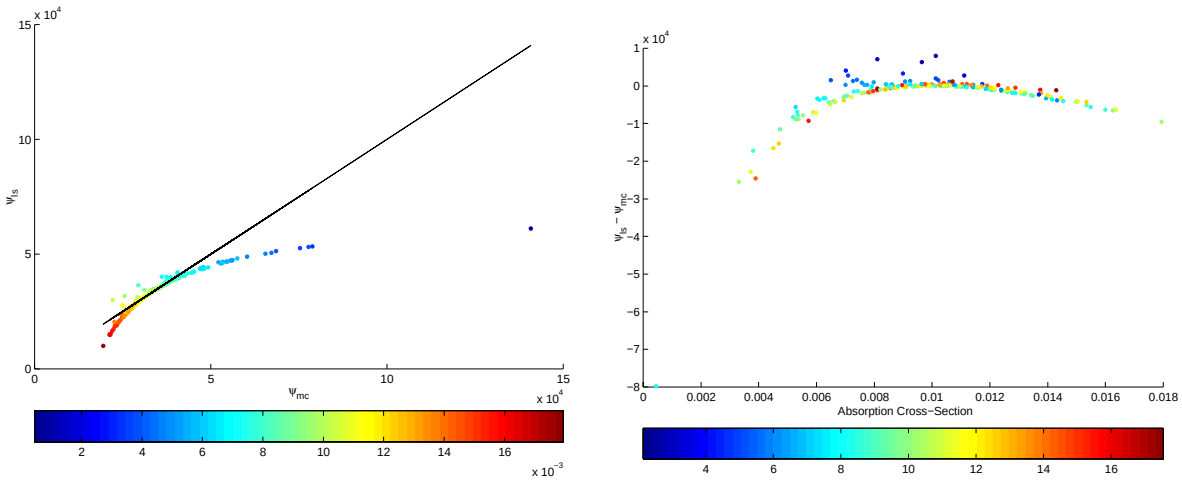

FIG. 6. Run-by-run correlation and differences between $\tilde{\psi}_{MC}$ and $\tilde{\psi}_{LS}$ for the diffusive test problem with an assumed cross section error of 30%. In (a), the dot color shows σ_a. In (b), the differences are ploted relative to σ_a and the dot color shows σ_s.

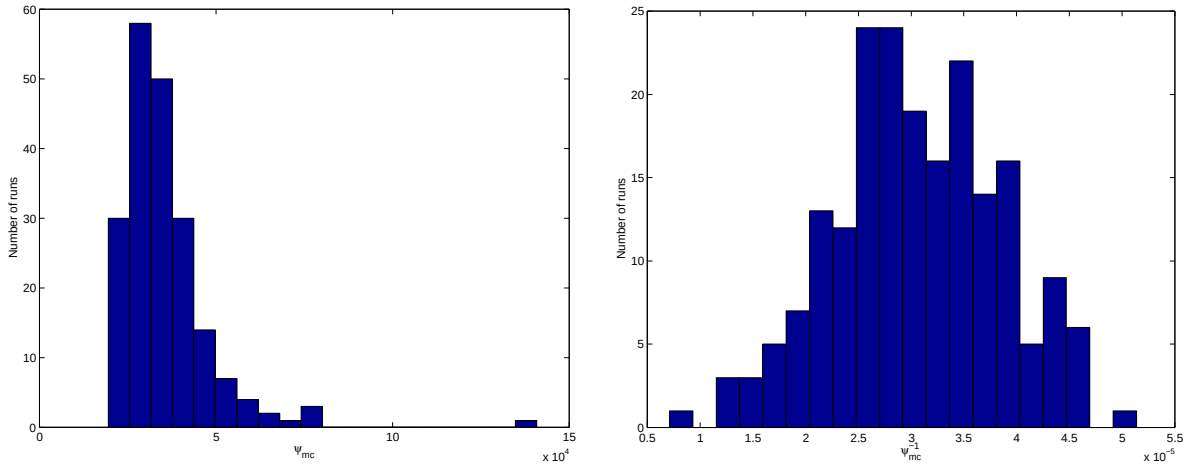

FIG. 7. Probability density functions for $\tilde{\psi}$ and $\tilde{\psi}^{-1}$ for the diffusive test problem with assumed cross section standard deviations of 30%.

TABLE 4
Comparison of means and standard deviations for the one-group diffusive test problem analyzed in terms of $\tilde{\psi}^{-1}$. $\tilde{\psi}^{-1}_{MC}$ were evaluated via full Monte Carlo runs. $\tilde{\psi}^{-1}_{LS}$ were evaluated via use of (13) and (10). The last column gives the percentage difference in the standard deviations estimated via the LS method relative to the standard deviation from the MC method.

Sample Std Dev	Number Samples	Nominal $\tilde{\psi}^{-1}$	Mean $\tilde{\psi}^{-1}_{MC}$	Mean $\tilde{\psi}^{-1}_{LS}$	Std Dev $\tilde{\psi}^{-1}_{MC}$	Std Dev $\tilde{\psi}^{-1}_{LS}$	Percent %Δ in Std Dev
10%	200	2.9909e-5	2.9962e-5	2.9909e-05	2.6190e-6	2.6201e-6	0.0418
20%	200	2.9909e-5	3.0138e-5	2.9909e-05	5.2420e-6	5.2401e-6	-0.0358
30%	200	2.9909e-5	3.0541e-5	2.9909e-05	7.9658e-6	7.8602e-6	-1.3254

When we compare the approximate probability density function for $\tilde{\psi}$ obtained from 250 runs with that for $\tilde{\psi}^{-1}$, the latter is much closer to being Gaussian. Both pdfs are shown in Figure 7. The form of these functions supports our supposition that it would be more accurate to do the LS expansion in terms of $\tilde{\psi}^{-1}$. The statistics in Table 4 and the correlation and error plots of Figure 8 show that the error in the estimate of the standard deviations has decreased from about 33% to about 1.3%, a result clearly demonstrating the applicability of the LS method to this problem.

6.3. Multigroup Test Problem Results

Our multigroup test problem solves a three energy group problem on a cube of length 30cm on a side. Reflecting boundaries are assumed on three adjoining faces, while vacuum Dirichlet conditions are used on the remaining three faces. The material used is pure aluminum at a density of 2.7g/cc. The energy group boundaries are given in Table 5. The source region is also a cube of length 10cm on a side situated in the corner of the larger cube where the three reflecting faces touch, and the source strength is identically constant within this smaller region and zero outside. The source strength is $10^7 \mathrm{n} \cdot \mathrm{cm}^{-2} \cdot \mathrm{s}^{-1}$. The preconditioning used consists of a block Gauss-Seidel structure in energy group, as there is only down-scattering for this problem, with each block inverse approximated via a DSA/sweeping-

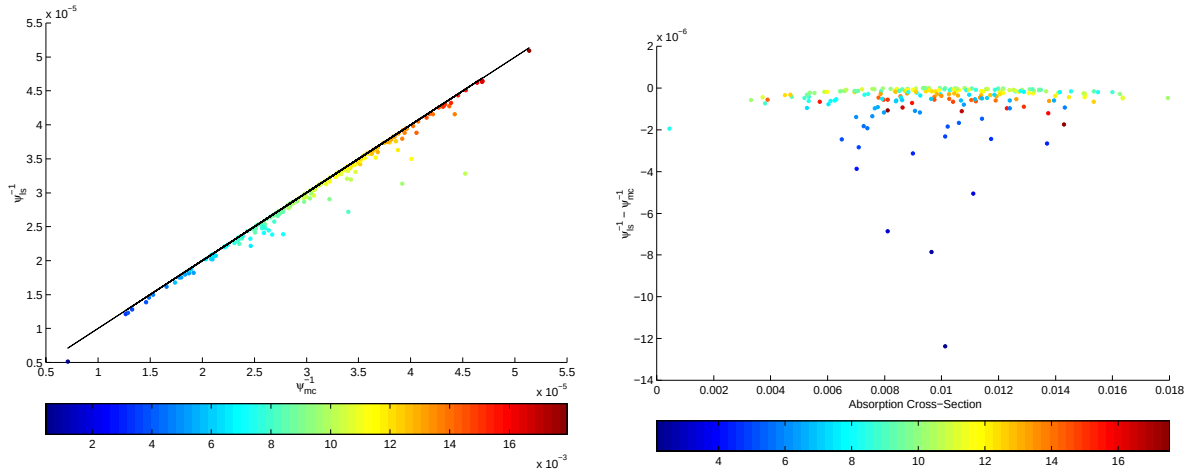

FIG. 8. Run-by-run correlation and differences between $\tilde{\psi}_{MC}^{-1}$ and $\tilde{\psi}_{LS}^{-1}$ for the diffusive test problem with an assumed cross section error of 30%. In (a), the dot color shows σ_a. In (b), the differences are ploted relative to σ_a and the dot color shows σ_s.

TABLE 5
Energy Group Boundaries for Multi-Group Test Problem (in MeV).

E_0	E_1	E_2	E_3
4.9659e0	3.6788e0	3.0119e0	1.9205e0

TABLE 6
Nominal Absorption Cross Sections for Multi-Group Test Problem (in cm^{-1}).

Group 0	Group 1	Group 2
7.58557e-04	2.51296e-04	2.04714e-05

based preconditioner. The nominal cross sections are given in Tables 6 and 7, and isotropic scattering is assumed. The spatial mesh is uniform of size $M = J = K = 20$ with S_4 quadrature (i.e., 24 directions).

Both a steady-state and a time-dependent problem were run. Figures 9 and 10 show the steady-state scalar flux for group 0 where the transparency in the plots is determined by the magnitude of the corresponding scaled sensitivity. The more sensitive the solution, the more opaque the slice planes are in the plots. For the time-dependent problem, the initial flux was identically zero, and the solution was integrated in time from 0 to 9.5×10^{-8} seconds, essentially run until a steady state was reached. Figures 11 through 16 show the time dependent history of three local detectors placed in the geometry along with upper and lower bounds obtained using the calculated scaled sensitivities with respect to either $\sigma_{a,0}$ or $\sigma_{s,0,0}$ as representative sensitivity calculations. If $d(t)$ is the detector value at time t and $s(t)$ the corresponding scaled sensitivity, then the upper and lower bounds are calculated using $d(t) + .15 \cdot s(t)$ for the upper bound and $d(t) - .15 \cdot s(t)$ for the lower bound. As σ_a appears directly in the definition of a detector, it is not surprising

TABLE 7
Nominal Scattering Cross Sections for Multi-Group Test Problem (in cm^{-1}).

Dest/Src	Group 0	Group 1	Group 2
Group 0	3.17672e-02	0.00000e+00	0.00000e+00
Group 1	1.92501e-02	3.01146e-02	0.00000e+00
Group 2	2.65110e-03	1.10446e-02	1.60951e-02

TABLE 8
Detector Region Boundaries for Multi-Group Test Problem.

Detector	XMIN	XMAX	YMIN	YMAX	ZMIN	ZMAX
1	55	60	55	60	55	60
2	45	50	40	50	40	50
3	40	45	40	45	40	45

TABLE 9
Statistics for Multi-Group Test Problem.

RUN	NST	NRE	NLI	Run Time (seconds)
Ψ only	492	1075	514	2182
Ψ and $\partial\Psi/\partial\sigma_{a,0}$ sensitivity	472	1340	816	4191
Ψ and $\partial\Psi/\partial\sigma_{s,0,0}$ sensitivity	511	1586	1015	4786

that the detector value would be more sensitive to σ_a rather than σ_s, and the plots reinforce this fact. The detector regions are defined in Table 8, and the cost and statistics for the time dependent calculations are given in Table 9. The counters in Table 9 are: NST = number of time steps, NRE = number of $F(t, \Psi, \dot{\Psi})$ evaluations, NLI = number of GMRES linear iterations, and the run time in seconds. The runs were all done using the IBM Blue Pacific machine at Lawrence Livermore National Laboratory. As can be seen from the run times, the cost of calculating the sensitivities is roughly twice that of the cost of performing the time dependent Ψ calculation.

6.3.1. Analysis of the Three-Group Steady-State Test Problem

For the three-group steady-state test problem, 250 LHS Monte Carlo (MC) runs were done for each of two uncertainty assumptions: one in which the nine non-zero cross sections of Tables 6 and 7 were sampled from Gaussian distributions for 10% standard deviations relative to their respective nominal values and one in which the errors were assumed to be 30%.

Our analysis of the steady-state uncertainty quantification is based on the integrated particle flux $\tilde{\psi}$ defined in (10). In Figure 17a, we confirm that the probability density function for $\tilde{\psi}$ is approximately Gaussian, indicating the potential of a good agreement between uncertainty quantification by use of linear sensitivities (LS) and uncertainty estimates by Monte Carlo (MC) methods. This conclusion follows directly from use of (13) to evaluate the LS estimates.

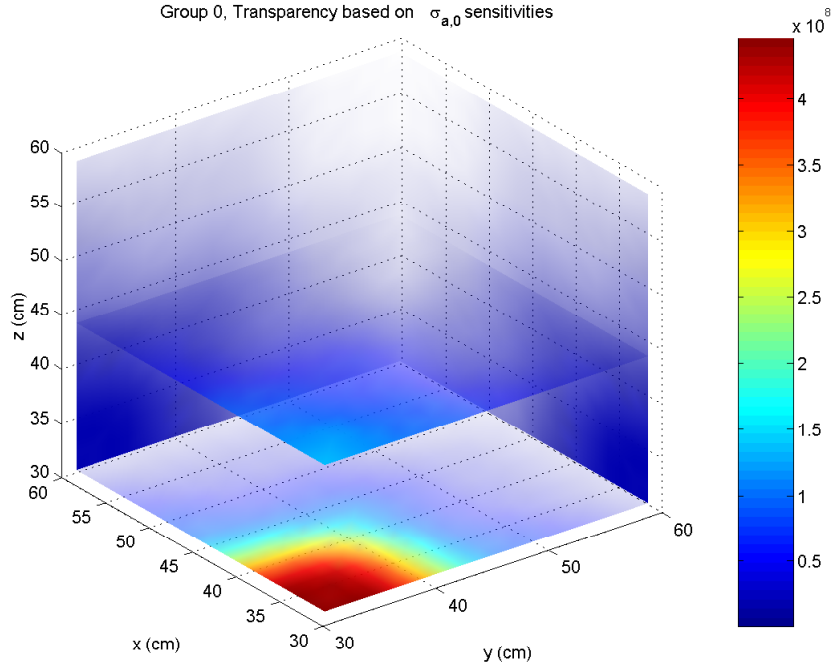

FIG. 9. Group 0 scalar flux for multigroup test problem showing scaled sensitivity with respect to $\sigma_{a,0}$.

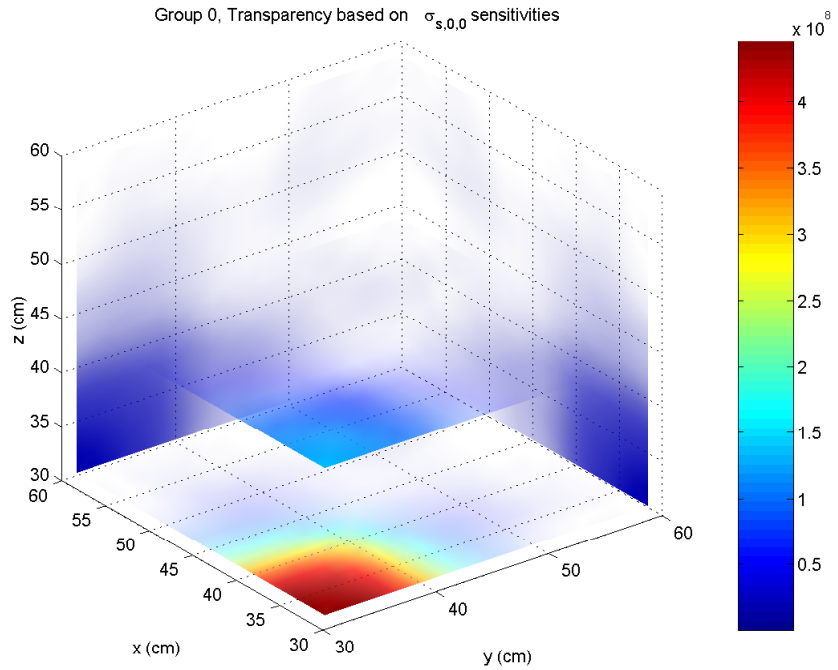

FIG. 10. Group 0 scalar flux for multigroup test problem showing scaled sensitivity with respect to $\sigma_{s,0,0}$.

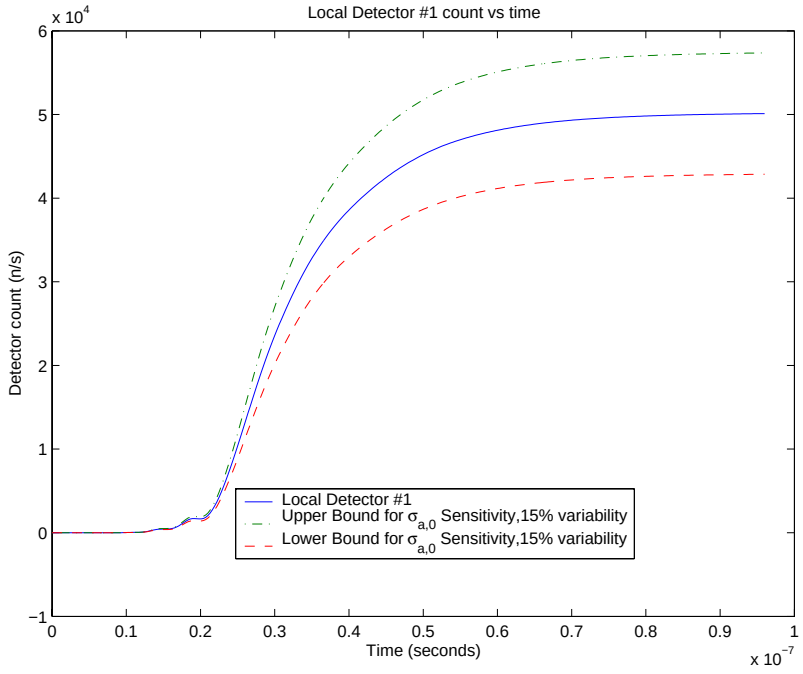

FIG. 11. Local detector #1 response with estimated error bounds obtained using the scaled $\sigma_{a,0}$ sensitivity.

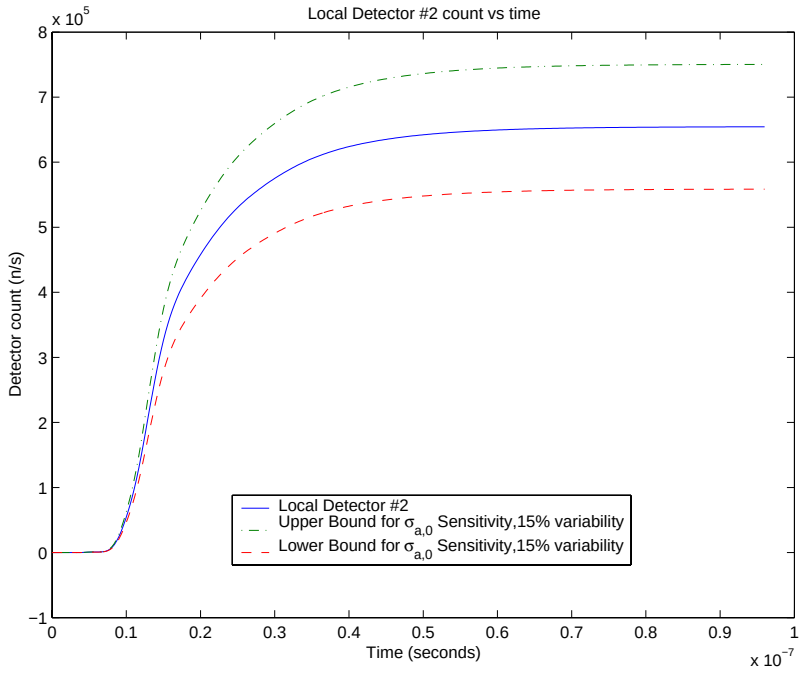

FIG. 12. Local detector #2 response with estimated error bounds obtained using the scaled $\sigma_{a,0}$ sensitivity.

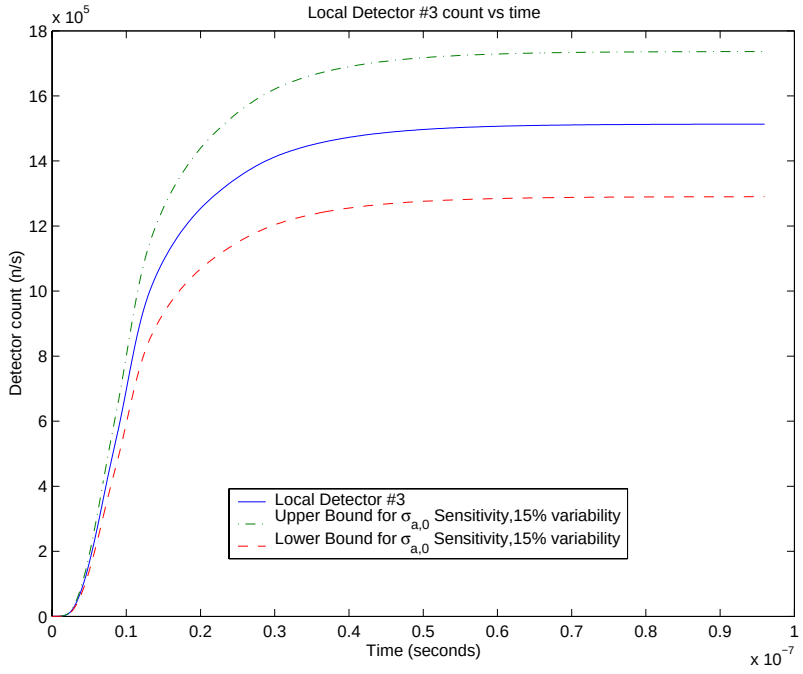

FIG. 13. Local detector #3 response with estimated error bounds obtained using the scaled $\sigma_{a,0}$ sensitivity.

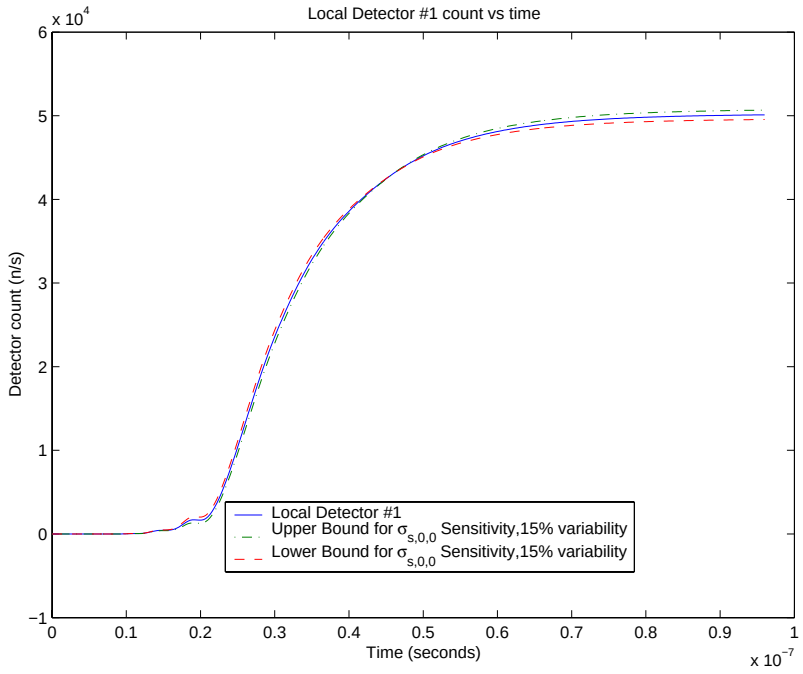

FIG. 14. Local detector #1 response with estimated error bounds obtained using the scaled $\sigma_{s,0,0}$ sensitivity.

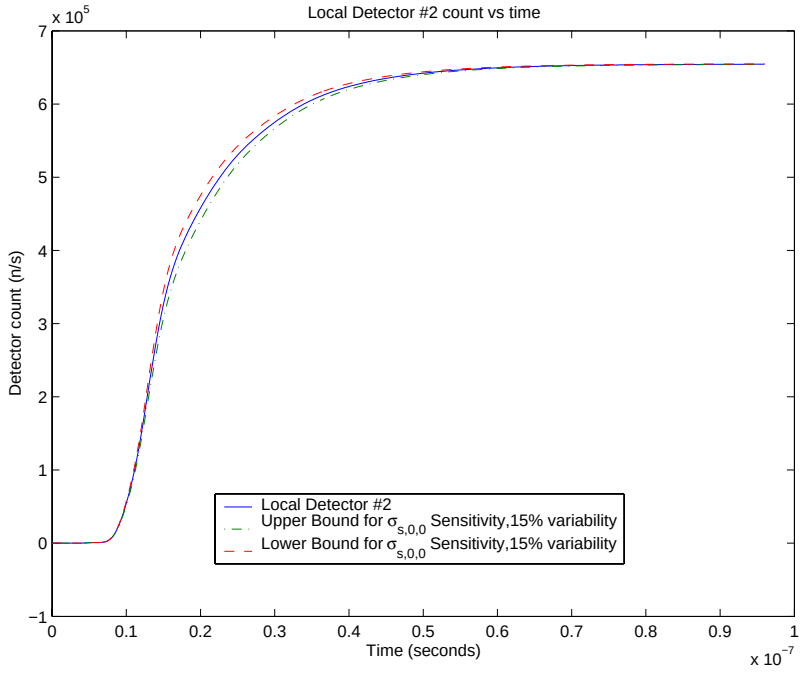

FIG. 15. Local detector #2 response with estimated error bounds obtained using the scaled $\sigma_{s,0,0}$ sensitivity.

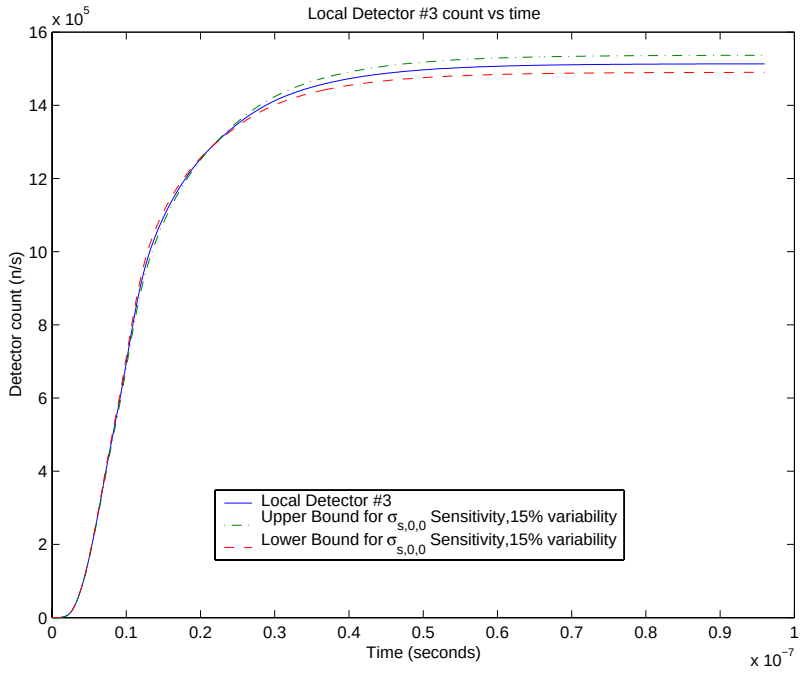

FIG. 16. Local detector #3 response with estimated error bounds obtained using the scaled $\sigma_{s,0,0}$ sensitivity.

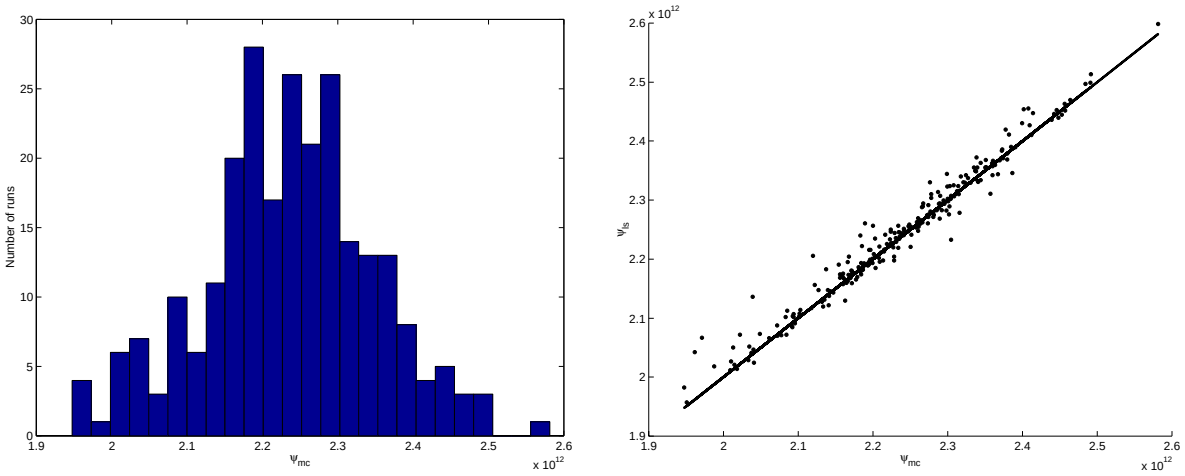

FIG. 17. (a) Probability density function for the integrated 3-Groups flux $\tilde{\psi}_{MC}$ for 250 Monte Carlo runs with assumed 30% cross section standard deviations. (b) Scatter plot of $\tilde{\psi}_{LS}$ relative to $\tilde{\psi}_{MC}$ for the same cases as in (a).

TABLE 10

Comparison of means and standard deviation for the three-group steady-state test problem. $\tilde{\psi}_{MC}$ were evaluated via full Monte Carlo runs. $\tilde{\psi}_{LS}$ were evaluated via use of (13) and (10). The last column gives the percentage difference in the standard deviations estimated via the LS method relative to the standard deviation from the MC method.

Sample Std Dev	Number Samples	Nominal $\tilde{\psi}$	Mean $\tilde{\psi}_{MC}$	Mean $\tilde{\psi}_{LS}$	Std Dev $\tilde{\psi}_{MC}$	Std Dev $\tilde{\psi}_{LS}$	Percent %Δ in Std Dev
10%	250	2.2434e+12	2.2425e+12	2.2433e+12	3.6940e+10	3.6931e+10	-2.3693e-02
30%	250	2.2434e+12	2.2364e+12	2.2432e+12	1.1289e+11	1.1079e+11	-1.8555e+00

Table 10 compares the mean and standard deviation of $\tilde{\psi}$ calculated from the MC results with the same statistics from the LS approximation. These data are shown for both the 10% and 30% cross section uncertainties. For the 10% case, the difference between the standard deviation estimates is negligible ($<$0.025%). For the 30% case, the corresponding difference is still small ($<$2%), indicating that the linear sensitivity approach remains quantitatively useful. To summarize the relationship between $\tilde{\psi}_{LS}$ and $\tilde{\psi}_{MC}$, Figure 17b presents a scatter plot for the 30% standard deviation case.

A contributing motivation for uncertainty quantification is determination of how to most effectively reduce the uncertainty in a diagnostic output such as $\tilde{\psi}$. By estimating the dependence of the total uncertainty on individual cross sections, guidance is gained on the greatest needs for reduction of the uncertainty in input parameters, either by further measurements or refinements in theoretical calculations. We compare the importance of individual cross sections in explaining the variance of $\tilde{\psi}$ in Table 11. The rows labeled "Corr" give Pearson's correlation coefficient between $\tilde{\psi}$ and the cross section in the column heading. This coefficient reflects the degree of linear relationship between two variables.

To compare differences between the MC and LS analyses, we have calculated the normalized sensitivities ($S/\tilde{\psi}_0$) from MC runs (S_{MC}) and direct solution of the sensitivity equations (S_{LS}). From our deterministic linear sensitivity

TABLE 11

This table presents two measures of the importance of individual cross sections in explaining the Monte Carlo (MC) variance of $\tilde{\psi}$ for the three-group test problem. Data are from 250 MC cases. The rows labeled "Corr" give Pearson's correlation coefficient between $\tilde{\psi}$ and the cross section in the column heading. This coefficient reflects the degree of linear relationship between two variables. The following rows present the normalized sensitivities ($S/\tilde{\psi}_0$) from least squares regression of MC runs (S_{MC}) and direct solution of the sensitivity equations (S_{LS}). $\tilde{\psi}_0$ is the nominal value of $\tilde{\psi}$. In calculating S_{MC}, linear regressions were passed through $\tilde{\psi}_0$ with the linear slope being the regressed sensitivity.

Corr/ Sens	Sample Std Dev	$\sigma_{a,0}$	$\sigma_{a,1}$	$\sigma_{a,2}$	$\sigma_{s,0,0}$	$\sigma_{s,0,1}$	$\sigma_{s,0,2}$	$\sigma_{s,1,1}$	$\sigma_{s,1,2}$	$\sigma_{s,2,2}$
Corr	10%	-8.939e-2	1.873e-2	-8.321e-2	7.659e-1	1.698e-1	-3.353e-1	5.577e-1	1.208e-1	1.472e-1
Corr	30%	-8.340e-2	9.689e-3	-7.995e-2	7.680e-1	1.556e-1	-3.298e-1	5.379e-1	1.128e-1	1.343e-1
S_{MC}	10%	-1.479e-2	3.071e-3	-1.363e-2	1.256e-1	2.768e-2	-5.613e-2	9.143e-2	1.988e-2	2.387e-2
S_{LS}	10%	-1.506e-2	-2.580e-3	-8.786e-5	1.389e-1	5.427e-2	-1.239e-3	7.436e-2	8.783e-3	2.542e-2
S_{MC}	30%	-1.405e-2	1.586e-3	-1.332e-2	1.281e-1	2.583e-2	-5.616e-2	8.967e-2	1.887e-2	2.221e-2
S_{LS}	30%	-1.506e-2	-2.580e-3	-8.786e-5	1.389e-1	5.427e-2	-1.239e-3	7.436e-2	8.783e-3	2.542e-2

calculations, we can immediately compute the sensitivity of $\tilde{\psi}$ to various cross sections by use of equations (13) and (10). In contrast, estimating the sensitivity of $\tilde{\psi}$ to individual cross sections from the Monte Carlo results requires least squares linear regression, the resulting slope being the desired sensitivity. In making these regressions, we have constrained the resulting lines to pass through $\tilde{\psi}_0 \equiv \tilde{\psi}(\bar{\sigma}_a, \bar{\sigma}_s)$, the nominal value of $\tilde{\psi}$. While it is beyond the scope of our analysis for this paper, we note that the sensitivities obtained from such regression analysis could be modified by use of different data weighting factors, giving more or less weight to outliers.

To illustrate the application of these sensitivities (both MC and LS) in the context of the total MC variance of $\tilde{\psi}$, Figure 18 contains plots of the estimated linear dependence of $\tilde{\psi}$ on $\sigma_{a,0}$ (a) and $\sigma_{s,0,0}$ (b). The red line, where distinct, shows the variation in $\tilde{\psi}$ based on the MC sensitivity estimate. The blue line is from use of the direct linear sensitivity (LS) calculations. In Figure 18a the MC and LS lines are essentially coincident.

7. CONCLUSIONS

We have presented a new method for the quantification of uncertainties of BTE solutions. Results on both one- and three-group test cases show that the resulting uncertainties differ from those computed using a Monte Carlo technique by only a fraction to a couple of percent. The new method requires computation of solution sensitivities during the solution computation. Solving for sensitivities along with solutions increases run time by a factor of 2-3, but gives a much faster uncertainty measure than the Monte Carlo method which requires hundreds of runs.

ACKNOWLEDGMENTS

The authors wish to thank Alan Hindmarsh for his many insightful comments during the development of the sensitivity variant of the BTE solver code. We also thank Alan Hindmarsh, Allan Taylor, and Steven Lee for the development of IDA and its sensitivity version.

REFERENCES

1. S. F. Ashby, P. N. Brown, M. R. Dorr, and A. C. Hindmarsh. A linear algebraic analysis of diffusion synthetic acceleration for the Boltzmann transport equation. *SIAM J. Numer. Anal.*, 32:128–178, 1995.

2. C. Bays and S. D. Durham. Improving a poor random number generator. *ACM Trans. on Math. Software*, 2(1):59–64, 1976.

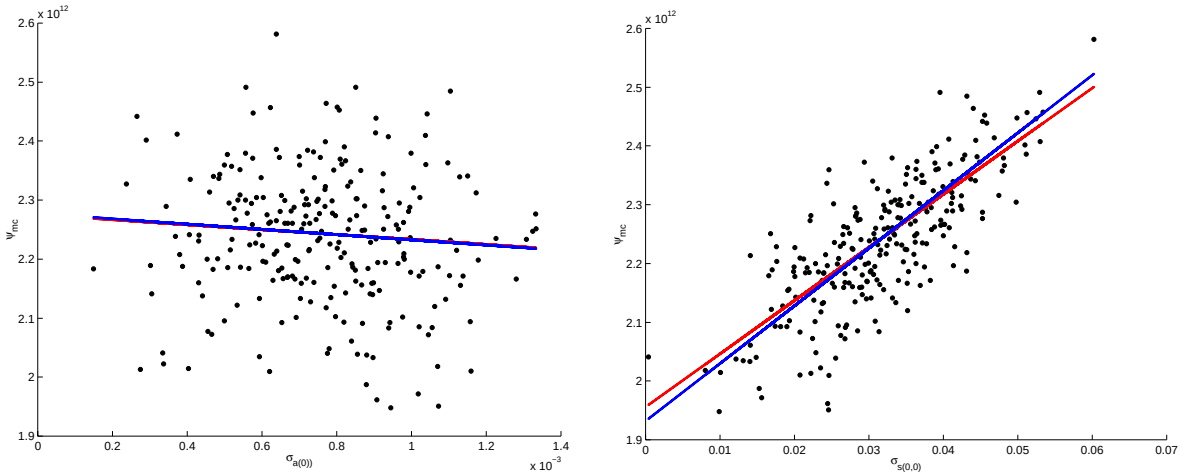

FIG. 18. (a) Linear dependence of $\tilde{\psi}$ on $\sigma_a\,,0$ for 250 Monte Carlo runs with assumed 30% cross section standard deviations. The linear sensitivity estimated from the MC runs by least squares regression (i.e., line slope) was used to produce the red line. The slope calculated using the sensitivity equations was used to produce the blue line. In both cases, the line is constrained to pass through the nominal values of $\tilde{\psi}$. (b) As for (a), but for the $\sigma_s\,,0\,,0$ cross section.

3. C. Bischof, L. Roh, and A. Mauer. ADIC — an extensible automatic differentiation tool for ANSI-C. *Software-Practice and Experience*, 27(12):1427–1456, 1997.
4. P. N. Brown. A linear algebraic development of diffusion synthetic acceleration for 3-D transport equations. *SIAM J. Numer. Anal.*, 32:179–214, 1995.
5. P. N. Brown and B. Chang. On the parallel solution of 3d time-dependent neutral particle transport calculations. Technical Report In preparation, Lawrence Livermore National Laboratory, Livermore, CA, 2001.
6. B. G. Carlson and K. D. Lathrop. Transport theory: The method of discrete ordinates. In H. Greenspan et al., editor, *Computing Methods in Reactor Physics*, pages 166–266, New York, 1968. Gordon and Breach.
7. R. H. Gardner, R. V. O'Neill, J. B. Mankin, and J. H. Carnery. A comparison of sensitivity analysis and error analysis based on a stream ecosystem model. *Ecological Modelling*, 12:173–190, 1981.
8. R. H. Gardner, J. R. Trabalka, and W. R. Emanuel. Methods of uncertainty analysis for a global carbon dioxide model. Technical Report DOE/OR/21400-4, Oak Ridge National Laboratory, 1985. Available from Publications Office, Environmental Sciences Division, Oak Ridge National Laboratory, Oak Ridge, Tennnessee 37831.
9. K. E. Grant, A. C. Hindmarsh, and A. G. Taylor. User documentation for SensKINSOL, a variant of KINSOL for sensitivity analysis. Manuscript in preparation.
10. J. M. Hammersley and D.C. Handscomb. *Monte Carlo Methods*. Chapman and Hall, London, 1964.
11. A. C. Hindmarsh and A. G. Taylor. User documentation for IDA, a differential-algebraic equation solver for sequential and parallel computers. Technical Report UCRL-MA-136910, Lawrence Livermore National Laboratory, 1999.
12. R. L. Iman and W.J. Conover. A distribution-free approach to inducing rank correlation among input variables. *Commun. Statist.-Simula. Computa.*, 11(3):311–334, 1982.
13. R. L. Iman and M. J. Shortencarier. A fortran 77 program and user's guide for the generation of latin hypercube and random samples for use with computer model. Technical Report SAND83-2365, Sandia National Laboratories, Albuquerque, New Mexico, 1984.
14. Ronald L. Iman, Jon C. Helton, and James E. Campbell. An approach to sensitivity analysis of computer models: Part 1 – introduction, input variable selection and preliminary variable assessment. *J. Quality. Tech.*, 13(3):174–183, July 1981.
15. M. H. Kalos and P. A. Whitlock. *Monte Carlo Methods — Volume I: Basics*. John Wiley & Sons, New York, 1986.
16. J. R. Koehler and A. B. Owen. Computer experiments. In S. Ghosh and C. R. Rao, editors, *Handbook of Statistics 13: Design and Analysis of Experiemnts*, pages 261–308. North-Holland, 1996.
17. S. Lee and A. C. Hindmarsh. User documentation for SensIDA, a variant of IDA for sensitivity analysis. Manuscript in preparation.
18. E. E. Lewis and W. F. Miller. *Computational Methods of Neutron Transport*. American Nuclear Society, La Grange Park, IL, 1993.

19. M. D. McKay, R.J. Beckman, and W.J. Conover. A comparison of three methods for selecting values of input variables in the analysis of output from a computer code. *Technometrics*, 21(2):239–245, 1979.

20. G. Palmiotti, M. Salvatores, and R. N. Hill. Sensitivity, uncertainty assessment, and target accuracies related to radiotoxity evaluation. *Nuclear Sci. and Eng.*, 117:239–250, 1994.

21. S. K. Park and K. W. Miller. Random number generators: Good ones are hard to find. *Comm. of the ACM*, 31(10):1192–1201, 1988.

22. Gerald C. Pomraning. *The Equations of Radiation Hydrodynamics*. Pergamon Press, Oxford, 1973.

23. A. G. Taylor and A. C. Hindmarsh. User documentation for KINSOL, a nonlinear solver for sequential and parallel computers. Technical Report UCRL-ID-131185, Lawrence Livermore National Laboratory, 1998.

University of California
Lawrence Livermore National Laboratory
Technical Information Department
Livermore, CA 94551